

Spectro-photometric Evolution of Elliptical Galaxies. II.

Models with Infall

R. Tantalo¹, C. Chiosi¹, A. Bressan², F. Fagotto^{3,1}

¹ Department of Astronomy, Vicolo dell' Osservatorio 5, 35122 Padua, Italy

² Astronomical Observatory, Vicolo dell' Osservatorio 5, 35122 Padua, Italy

³ Instituto de Astrofísica de Canarias, 38200 La Laguna, Tenerife, Spain

Received July 1995, accepted

Abstract. In this paper we present new chemo-spectro-photometric models of elliptical galaxies in which infall of primordial gas is allowed to occur. They aim to simulate the collapse of a galaxy made of two components, i.e. luminous material and dark matter. The mass of the dark component is assumed to be constant in time, whereas that of the luminous material is supposed to accrete at a suitable rate. They also include the effect of galactic winds powered by supernova explosions and stellar winds from massive, early-type stars. The models are constrained to match a number of properties of elliptical galaxies, i.e. the slope and mean colours of the colour-magnitude relation (CMR), V versus $(V-K)$, the UV excess as measured by the colour $(1550-V)$ together with the overall shape of the integrated spectral energy distribution (ISED) in the ultraviolet, the relation between the Mg_2 index and $(1550-V)$, the mass to blue luminosity ratio M/L_B as a function of the B luminosity, and finally the broad-band colours $(U-B)$, $(B-V)$, $(V-I)$, $(V-K)$, etc. The CMR is interpreted as a mass-metallicity sequence of old, nearly coeval objects, whose mean age is 15 Gyr. Assuming the law of star formation to be proportional to $M_g^k(t)$ with $k = 1$, the rate of star formation as function of time starts small, grows to a maximum, and then declines thus easily avoiding the excess of metal-poor stars found by BCF with the closed-box scheme (the analog of the G-Dwarf Problem in the solar vicinity). Owing to their stellar content, infall models can easily reproduce all the basic data of the galaxies under examination. As far as the UV excess is concerned, the same sources proposed by BCF are found to hold also with the infall scheme. H-HB and AGB manqué stars of high metallicity play the dominant role, and provide a robust explanation of the correlation between the $(1550-V)$ colour and the luminosity, mass and metallicity of the galaxies. Furthermore, these models con-

firm the potential of the $(1550-V)$ colour as an age indicator in cosmology as already suggested by BCF. In the rest frame of a massive and metal-rich elliptical galaxy, this colour suffers from one major variation: at the onset of the so-called H-HB and AGB-manqué stars (age about 5.6 Gyr). This transition occurs at reasonably small redshifts and therefore could be detected with the present-day instrumentation.

Key words: Galaxies: ellipticals – Galaxies: evolution – Galaxies: stellar content

1. Introduction

Bressan et al. (1994, BCF) have recently presented chemo-spectro-photometric models for elliptical galaxies that were particularly designed to match the UV excess observed in these systems (Burstein et al. 1988) together with its dependence on the galaxy luminosity, mass, metallicity, Mg_2 index, and age. In brief, BCF models stand on the closed-box approximation and the enrichment law $\Delta Y/\Delta Z = 2.5$, allow for the occurrence of galactic winds powered by the energy input from supernovae and stellar winds from massive stars, and use the CMR of elliptical galaxies in Virgo and Coma clusters (Bower et al. 1992a,b) as one of the main constraints.

In the BCF models the history of star formation consists of an initial period of activity followed by quiescence after the onset of the galactic winds, whose duration depends on the galactic mass, being longer in the high mass galaxies and shorter in the low mass ones. With the adoption of the closed-box description of chemical evolution, the maximum efficiency of star formation occurred at the very initial stage leading to a metallicity distribution in the models (relative number of stars per metallicity interval) skewed towards low metallicities.

*
Send offprint requests to: C. Chiosi

The comparison of the theoretical integrated spectral energy distribution (ISED) of the models with those of prototype galaxies with different intensity of the UV excess, for instance NGC 4649 with strong UV emission and $(1550-V) \sim 2.24$ and NGC 1404 with intermediate UV excess and $(1550-V) \sim 3.30$, indicated that a good agreement was possible but for the region 2000 Å to about 3500 Å where the theoretical ISED exceeded the observed one.

the closed-box models the contribution to the ISED from stars in different metallicity bins. Looking at the paradigmatic case of the ISED of NGC 4649, BCF found that this can be matched by a mix of stellar populations in which no stars with metallicity lower than $Z = 0.008$ are present. The results of these experiments are shown here in Fig. 1 for the sake of clarity.

It goes without saying that one may attribute the discrepancy of predicted and observed spectra in the region 2000 to 3500 Å to uncertainties in the theoretical spectra. However, the following considerations can be made. Firstly, those experiments clarified that the main contributors to the excess of flux are the turn-off stars of low metallicity ($0.0004 \leq Z \leq 0.008$) whose effective temperature at the canonical age of 15 Gyr ranges from 6450 K to 5780 K. Secondly, the Kurucz (1992) spectra (at the base of the library adopted by BCF) fit the Sun and Vega, two stars of different metallicity but whose effective temperatures encompass the above values. Finally, the disagreement in question implies that the theoretical spectra overestimate the flux in this region by a factor of about 4, which is hard to accept. On the basis of the above arguments BCF concluded that the excess is real and that the discrepancy in question is the analog of the classical G-Dwarf Problem in the solar vicinity.

In brief, it has long been known that the closed-box model applied to study the chemical history of the solar vicinity fails to explain the metallicity distribution observed among the old field stars, giving rise to the so-called G-Dwarf Problem (Tinsley 1980a,b). The solution of the G-Dwarf dilemma are models with infall (Lynden-Bell 1975, Tinsley 1980a, Chiosi 1981), i.e. models in which the total mass of the disk is let increase with time at a convenient rate starting from a much lower value. With the current law of star formation (proportional to the gas mass) the competition between gas accretion by infall and gas depletion by star formation gives rise to a non monotonic time dependence of the star formation rate which instead of steadily decreasing from the initial stage as in the closed-box model starts small, increases to a peak value, and then declines over a time scale which is a sizeable fraction of the infall time scale. The advantage of the infall model with respect to the closed-box one, is that the metallicity increases faster, and very few stars are formed at very low metallicity. Since the excess of very low-metal stars is avoided, the G-Dwarf Problem is naturally solved.

Applied to an elliptical galaxy, the infall model of chemical evolution can closely mimic the collapse of the parental proto-galaxy from a very extended size to the one we see today. Plausibly, as the gas falls into the gravitational potential well at a suitable rate and the galaxy shrinks, the gas density increases so that star formation begins. As more gas flows in, the more efficient star formation gets. Eventually, the whole gas content is exhausted and turned into stars, thus quenching further star formation. Like in the disk, the star formation rate starts small,

Fig. 1. The observed spectrum of the elliptical galaxy NGC 4649 (filled squares) kindly provided by L. Buson (1995, private communication). The vertical bars show the global error on the $(1550-V)$ colours from Burstein et al. (1988). The two lines show theoretical spectra for the galactic model of BCF with $M_L = 3^{12} M_\odot$ characterized by the parameters $k = 1$, $\nu = 20$ and $\zeta = 0.40$ and age of 15 Gyr, obtained with different assumptions concerning the contribution from stars in different metallicity bins. The solid line is the regular spectrum in which all the components are present. Note the discrepancy in the wavelength interval 2000 - 4000 Å. The dashed line is the same but without the contribution from all stars with metallicity $Z \leq 0.008$. Note the agreement reached in this case. All the spectra are normalized to coincide in the flux at 5000 Å.

The analysis of the reason of disagreement led BCF to conclude that this is a consequence of the closed-box approximation. Indeed this type of model is known to predict an excess of low-metal stars. The feature is intrinsic to the model and not to the particular numerical algorithm used to follow the chemical history of a galaxy.

In order to check their suggestion, BCF performed several numerical experiments in which they artificially removed from the mix of stellar populations predicted by

risers to a maximum, and then declines. Because of the more efficient chemical enrichment of the infall model, the initial metallicity for the bulk of star forming activity is significantly different from zero.

In this paper, we present simple models of spectro-photometric evolution of elliptical galaxies whose chemical enrichment is governed by the infall scheme, i.e. models in which the mass of the galaxy is let increase with time. Models of this type are consistent with the chemodynamical models by Theis et al. (1992) and are advocated by Phillips (1993) to interpret the galaxy counts at faint magnitudes, which are known to exceed those expected from standard evolutionary models with an initial spike of star formation followed by quiescence.

As in BCF, the models (both chemical and spectro-photometric) are constrained to reproduce at the same time a number of key features of elliptical galaxies, namely the slope and mean colours of the CMR, V versus $(V-K)$, for the galaxies in the Virgo and Coma clusters, the UV excess as measured by the colour $(1550-V)$ together with the overall ISED, the relation between the Mg_2 index and $(1550-V)$, the mass to blue luminosity ratio M/L_B as a function of the B luminosity, and finally the present broad band colours $(U-B)$, $(B-V)$, $(V-I)$, $(V-K)$, etc.

The CMR is from Bower et al. (1992a,b), the data on the UV excess and Mg_2 -(1550- V) relationship are from Burstein et al. (1988), and the data on the ratio M/L_B are from Bender et al. (1992,1993) and Terlevich & Boyle (1993) for $H_0 = 50 \text{ km sec}^{-1} \text{ Mpc}^{-1}$.

There is one aspect of the problem that should be clarified in advance. The bottom line of BCF models is the interpretation of the Virgo and Coma cluster CMR as a mass-metallicity sequence whose slope is driven by the onset of galactic winds (cf. Larson 1974; Saito 1979a,b; Vader 1986; Arimoto & Yoshii 1986; Matteucci & Tornambé 1987; Angeletti & Giannone 1990; Padovani & Matteucci 1993) and whose tightness is the signature of old ages with small dispersion, $13 \div 15 \text{ Gyr}$ according to Bower et al. (1992a,b).

In contrast, the CMR for nearby galaxies in small groups and field is more dispersed than the one for the Virgo and Coma clusters suggesting that elliptical galaxies may originate from the mergers of spiral galaxies spread over several billion years (Schweizer & Seitzer 1992; Alfensleben & Gerhard 1994; Charlot & Silk 1994). Also in this case the CMR implies the existence of a suitable mass-metallicity sequence.

Therefore, the view that elliptical galaxies are primordial old objects with a dominant initial burst of activity may co-exist with the view that many if not all of them are the result of mergers implying more recent star formation activities that may vary from galaxy to galaxy.

How the different interpretation of the CMR affects the use of this as a constraint on our models? This question has been addressed by Bressan et al. (1995, BCT), who showed that the slope and the mean colours of the

CMR are compatible with both alternatives, thus validating its ability to constrain the models. Therefore, owing to its better definition, we adopt the Bower et al. (1992a,b) CMR and assume that it is made of nearly coeval objects with mean age of about 15 Gyr. Strictly speaking the models below are best suited to cluster elliptical galaxies. The analysis of the merger scenario is beyond the scope of this study.

Section 2 reports on the new spectral library adopted to calculate the spectro-photometric models presented in this paper. Section 3 describes the properties of Single Stellar Populations (SSP) calculated with the new spectral library above. Section 4 outlines the chemical models in usage. Section 5 contains closed-box models calculated with the new spectral library and compares them with those of BCF. It is found that no closed-box model can match all the imposed constraints. Section 6 is the same but for infall models. Section 7 presents the results of the chemical and spectro-photometric models with infall and describes in detail the properties of the models with different mass. In particular we examine the CMR, the mass to blue luminosity ratio M/L_B , the UV excess and accompanying $(1550-V)$ versus Mg_2 relation, the evolution of the broad-band colours as a function of the age, and the potential capability of the $(1550-V)$ colour of being a good age indicator in cosmology. Finally, Section 8 contains a few concluding remarks.

2. A new spectral library

The library of stellar spectra adopted in this study is very similar to the one used by BCF. There are however a few important changes deserving a bit of explanation.

The main body of the spectral library is from R. Kurucz (1992), however extended to the high and low temperature ranges. For stars with high $T_{\text{eff}} > 50,000 \text{ K}$ pure black-body spectra are assigned, whereas for stars with $T_{\text{eff}} < 3500 \text{ K}$ the new catalog of stellar fluxes by Fluks et al. (1994) is adopted (see Silva 1995 for details). This catalog includes 97 observed spectra for all M-spectral subtypes in the wavelength range $3800 \leq \text{\AA} \leq 9000$, and synthetic photospheric spectra in the range $9900 \leq \text{\AA} \leq 12500$.

The scale of T_{eff} in Fluks et al. (1994) is similar to that of Ridgway et al. (1980) for spectral types earlier than M4 but deviates from it for later spectral types. Since Ridgway's et al. (1980) scale does not go beyond the spectral type M6, no comparison for more advanced spectral types is possible.

The problem is further complicated by possible effects of metallicity. The Ridgway scale of T_{eff} is based on stars with solar metallicity ($Z \sim 0.02$) and empirical calibrations of the T_{eff} -scale for $Z \neq 0.02$ are not available. In contrast, the library of SSPs span the range of metallicity $0.0004 \leq Z \leq 0.1$.

To cope with this difficulty, we have introduced the metallicity- T_{eff} relation of Bessell et al. (1989,1991) using the (V-K) colour as a temperature indicator. An interpolation is made between the T_{eff} of Bessell et al. (1989) and the (V-K) colours given by Fluks et al. (1994) for the spectral types from M0 to M10.

Figure 2 compares the T_{eff} scales of Ridgway et al. (1980), Fluks et al. (1994) and Bessell et al. (1989, 1991) with the one we have obtained. This latter is also given in Table 1 as a function of the spectral type and metallicity. Column (1) is the spectral type, column (2) is the (V-K) colour from Fluks et al. (1994) for solar metallicity, column (3) through (6) are the T_{eff} for different metallicities ($Z=0.06$, $Z=0.02$, $Z=0.006$, $Z=0.002$) as indicated.

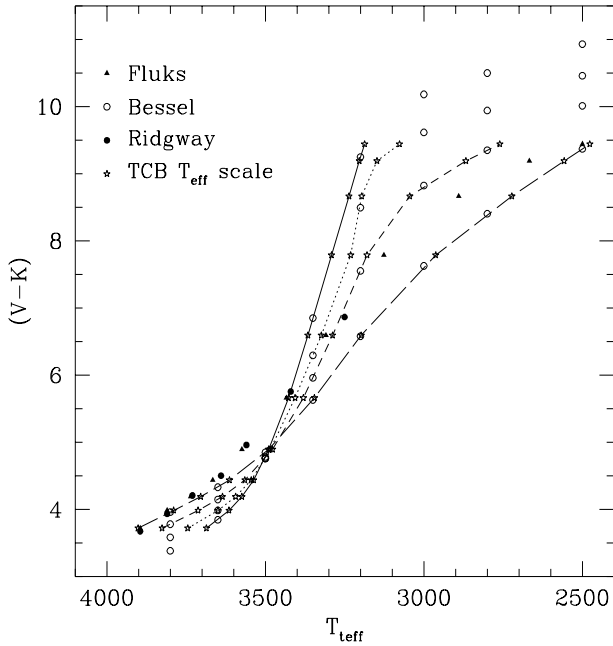


Fig. 2. Four (V-K) versus T_{eff} scales: Ridgway et al. (1980) — full dots, Bessell et al. (1989, 1991) — open dots, Fluks et al. (1994) for solar metallicity — solid triangles. Finally, the asterisks correspond to our data. The lines show the interpolations between the (V-K) colours of Fluks et al. (1994) and the T_{eff} scales of Bessell et al. (1989, 1991) for different metallicities

3. A new library of SSPs with $\Delta Y/\Delta Z=2.5$

BCF presented an extended library of integrated magnitudes and colours of SSPs as a function of the age for several combinations of the chemical parameters Y (helium) and Z (metallicity) obeying the enrichment law $\Delta Y/\Delta Z = 2.5$ (Pagel 1989, Pagel et al. 1992). The sets of chemical abundances were $[Y=0.230, Z=0.0004]$, $[Y=0.240, Z=0.004]$, $[Y=0.250, Z=0.008]$,

Table 1. Spectral type, (V-K) colour, and T_{eff} scales as a function of the metallicity

SpT	(V-K)	$T_{0.06}$	$T_{0.02}$	$T_{0.006}$	$T_{0.002}$
M0	3.722	3686	3745	3825	3902
M1	3.986	3615	3650	3712	3789
M2	4.190	3574	3594	3636	3704
M3	4.439	3537	3545	3565	3613
M4	4.895	3489	3484	3477	3490
M5	5.662	3427	3406	3380	3345
M6	6.595	3366	3324	3288	3198
M7	7.789	3291	3231	3179	2963
M8	8.667	3236	3196	3044	2722
M9	9.192	3204	3148	2868	2558
M10	9.444	3187	3077	2760	2476

$[Y=0.280, Z=0.020]$, $[Y=0.352, Z=0.05]$, and $[Y=0.475, Z=0.1]$.

The stellar models used to calculate the SSPs with $\Delta Y/\Delta Z = 2.5$ in BCF were from Alongi et al. (1993), Bressan et al. (1993) and Fagotto et al. (1994a,b,c). They span the mass range from 0.6 to $120M_{\odot}$ and go from the zero age main sequence until the start of the thermally pulsing asymptotic giant branch stage (TP-AGB) or C-ignition as appropriate to the initial mass of the star.

In this paper we adopt the same library of stellar models to calculate our SSPs however with two major differences with respect to BCF. First we extend the zero age main sequence down to $0.15M_{\odot}$ using the VanderBerg (1985) library of low mass stars (the lowest mass in BCF was $0.6M_{\odot}$). Second we increase the mass loss parameter η governing stellar winds from RGB and AGB stars from $\eta = 0.35$ to $\eta=0.45$ (see BCF for more details).

The method of SSP calculation is exactly the same as in BCF, to whom we refer for all details. Suffice it to recall that SSP models are for the IMF expressed by equations (15) below, with slope $x = 2.35$ and lower and upper limits of integration, $M_L = 0.15M_{\odot}$ and $M_U = 120M_{\odot}$ respectively. It is worth recalling that the integrated magnitudes of these ideal SSPs must be properly scaled when applied to real SSPs (for instance star clusters).

Table 2 contains the integrated magnitudes and colours of the new SSPs for different values of the age. We list the age in Gyr (column 1), the absolute visual magnitude M_V (column 2), the absolute bolometric magnitude M_{bol} (column 3), the bolometric corrections BC (column 4), and the colours (U-B), (B-V), (V-R), (R-I), (V-J), (V-K), (V-L), (V-M), (V-N), and (1550-V), columns (5) through (14), respectively.

Figure 3 shows the temporal evolution of four selected colours, namely (U-B), (B-V), (V-J) and (V-K) for three SSPs with different chemical composition: Panel (a) for $[Y=0.28, Z=0.02]$, Panel (b) for $[Y=0.25, Z=0.008]$, and

Panel (c) for $[Y=0.23 \text{ } Z=0.0004]$. The vertical arrows show the ages at which a sudden variation in the colours caused by the onset of AGB and RGB stars is expected to occur according to Renzini & Buzzoni (1986).

Figures 4 and 5 display the temporal evolution of the colours (V–K) and (1550–V), respectively, for all the chemical compositions under consideration. While the (V–K) colour remains almost constant for SSPs older than 5 Gyr (cf. Fig.4), the (1550–V) colour (Fig. 5) undergoes large variations. This implies that in order to match the observed integrated (V–K) and (1550–V) colours, the galactic models (both closed and open) must develop suitable mean and maximum metallicities (see below).

4. Chemical models of elliptical galaxies

4.1. Outline of the Model

The model aims at simulating in a very simple fashion the formation of an elliptical galaxy by collapse of primordial gas in presence of dark matter. To this scope, elliptical galaxies are described as one-zone models made of two components, luminous material of mass $M_L(t)$ embedded in a halo of dark matter of mass M_D , whose presence affects only the gravitational potential of the galaxy and the binding energy of the gas.

In the infall scheme the mass of the luminous component (supposedly in form of gas) is let increase with time according to

$$\frac{dM_L(t)}{dt} = \dot{M}_0 \exp(-t/\tau) \quad (1)$$

where τ is the accretion time scale.

The constant \dot{M}_0 is obtained from imposing that at the galaxy age T_G the value $M_L(T_G)$ is reached:

$$\dot{M}_0 = \frac{M_L(T_G)}{\tau[1 - \exp(-T_G/\tau)]} \quad (2)$$

Therefore, integrating the accretion law the time dependence of $M_L(t)$ is

$$M_L(t) = \frac{M_L(T_G)}{[1 - \exp(-T_G/\tau)]} [1 - \exp(-t/\tau)] \quad (3)$$

The spatial distribution of the dark component with respect to the luminous one is supposed to obey the dynamical models of Bertin et al. (1992) and Saglia et al. (1992) in which the mass and radius of the dark component, M_D and R_D , respectively, are related to those of the luminous material, M_L and R_L , by the relation

$$\frac{M_L(t)}{M_D} \geq \frac{1}{2\pi} \left(\frac{R_L(t)}{R_D} \right) [1 + 1.37 \left(\frac{R_L(t)}{R_D} \right)] \quad (4)$$

The mass of the dark component is assumed be constant in time and equal to $M_D = \beta M_L(T_G)$ with $\beta = 5$.

Fig. 3. Panel (a): The colour evolution of a SSP with composition $[Y=0.28 \text{ } Z=0.02]$. Note the large variation in the red colours caused by the onset of AGB stars at the age $t(M_{UP})$. The appearance of RGB stars expected to occur at the age $t(M_{HeF})$ is masked by AGB stars so that no change in the colour is noticed. Ages are in years. **Panel (b):** The same as in Panel (a) but for a SSP with composition $[Y=0.25 \text{ } Z=0.008]$. **Panel (c):** The same as in Panel (a) but for a SSP with composition $[Y=0.23 \text{ } Z=0.0004]$

Furthermore, the binding gravitational energy of the gas is given by

$$\Omega_g(t) = -\alpha_L G \frac{M_g(t)M_L(t)}{R_L(t)} - G \frac{M_g(t)M_D}{R_L(t)} \Omega'_{LD} \quad (5)$$

where $M_g(t)$ is the current value of the gas mass, α_L is numerical factor $\simeq 0.5$, and

$$\Omega'_{LD} = \frac{1}{2\pi} \left(\frac{R_L(t)}{R_D} \right) [1 + 1.37 \left(\frac{R_L(t)}{R_D} \right)] \quad (6)$$

is the contribution to the gravitational energy given by the presence of dark matter. Following Bertin et al. (1992)

and Saglia et al. (1992) in the above relations we assume $M_L/M_D = 0.2$ and $R_L/R_D = 0.2$.

In order to apply the above equations for the binding gravitational energy of the gas to a model galaxy we need a relation between the radius and the mass of the luminous component. To this aim, we start noticing that with the assumed ratios M_L/M_D and R_L/R_D the contribution to gravitational energy by the dark matter is $\Omega'_{LD} = 0.04$ and the total correction to the gravitational energy of the gas (eq. 5) does not exceed 0.3 of the term for the luminous mass.

Given these premises, and assuming that at each stage of the infall process the amount of luminous mass that has already accumulated gets soon virialized and turned into stars, we can approximate the total gravitational energy and radius of the material already settled onto the equilibrium configuration with the relations for the total gravitational energy and radius as function of the mass (in this case $M_L(t)$) obtained by Saito (1979a,b) for elliptical galaxies whose spatial distribution of stars is such that the global luminosity profile obeys the $R^{1/4}$ law. In such a case the relation between $R_L(t)$ and $M_L(t)$ is

$$R_L(t) = 26.1 \times (M_L(t)/10^{12}M_\odot)^{(2-\eta)} \text{ kpc} \quad (7)$$

with $\eta = 1.45$ (cf. also Arimoto & Yoshii 1987).

Finally, another useful quantity is the volume density of gas $\rho_g(t)$ given by

$$\rho_g(t) = \frac{3M_g(t)}{4\pi R_L(t)^3} \quad (8)$$

It is worth recalling that if dark and luminous matter are supposed to have the same spatial distribution, equations (5) and (6) are no longer required. Indeed, the binding energy of the gas can be simply obtained from the total gravitational energy of Saito (1979b) provided that the mass $M_L(t)$ is replaced by the sum $M_L(t) + M_D$. In such a case, the binding energy of the gas is

$$\Omega_g(t) = \Omega_{L+D}(t)M_g(t)[2 - M_g(t)]. \quad (9)$$

4.2. Basic Equations of Chemical Evolution

Denoting with $X_i(t)$ the current mass abundance of an element i and introducing the dimensionless variables

$$G(t) = M_g(t)/M_L(T_G) \quad (10)$$

and

$$G_i(t) = G(t)X_i(t), \quad (11)$$

the equations governing the time variation of the $G_i(t)$ and hence $X_i(t)$ are

$$\frac{dG_i(t)}{dt} = -X_i(t)\Psi(t) +$$

Fig. 4. The temporal evolution of the (V-K) colour for SSPs with different chemical compositions obeying the enrichment law $\Delta Y/\Delta Z = 2.5$

Fig. 5. The temporal evolution of the (1550-V) colour for SSPs with different chemical compositions obeying the enrichment law $\Delta Y/\Delta Z = 2.5$

$$\int_{M_L}^{M_U} \Psi(t - t_M) \phi(M) Q_i(t - t_M) dM + \frac{d[G_i(t)]_{\text{inf}}}{dt} \quad (12)$$

where $\Psi(t)$ is the rate of star formation in units of $M_L(T_G)$, t_M is the lifetime of a star of mass M , $\Phi(M)$ is the initial mass function, $Q_i(t - t_M)$ is the fraction of mass ejected by such a star in form of an element i , and $[G_i(t)]_{\text{inf}}$ is the rate of gas accretion. This is expressed by

$$\frac{d[G_i(t)]_{\text{inf}}}{dt} = \frac{X_{\text{inf}}}{M_g(t)} \frac{dM(t)}{dt} \quad (13)$$

By definition $\sum_i X_i(t) = 1$. All the details of the $Q_i(t - t_M)$ are omitted here for the sake of brevity. They can be found in Chiosi (1986) and Matteucci (1991) to whom the reader should refer.

The stellar birth rate, i.e. the number of stars of mass M born in the interval dt and mass interval dM is:

$$dN = \Psi(t, Z) \phi(M) dM dt \quad (14)$$

where $\Psi(t)$ is the rate of star formation as a function of time and enrichment, while $\phi(M)$ is the initial mass function (IMF).

The IMF is the Salpeter law expressed as

$$\phi(M) = M^{-x} \quad (15)$$

where $x = 2.35$. The IMF is normalized by choosing the parameter ζ

$$\zeta = \frac{\int_{M_*}^{M_U} \phi(M) \times M \times dM}{\int_{M_L}^{M_U} \phi(M) \times M \times dM} \quad (16)$$

i.e. the fraction of total mass in the IMF above M_* , and deriving the lower limit of integration M_L . The upper limit of integration is $M_U = 120M_\odot$, the maximum mass in our data base of stellar models, while the mass limit M_* is the minimum mass contributing to the nucleosynthetic enrichment of the interstellar medium over a time scale comparable to the total lifetime of a galaxy. This mass is approximately equal to $1M_\odot$.

4.3. Star Formation Rate

The rate of star formation is assumed to depend on the gas mass according to

$$\Psi(t) = \nu M_g(t)^k \quad (17)$$

where ν and k are adjustable parameters. The star formation rate normalized to $M_L(T_G)$ becomes

$$\Psi(t) = \nu M_L(T_G)^{k-1} G(t)^k \quad (18)$$

Linear and quadratic dependencies of the star formation rate on the gas content, $k = 1$ and $k = 2$ respectively, were first proposed by Schmidt (1959) and have

been adopted ever since because of their simplicity (see Larson 1991 for a recent review).

With the law of star formation of equation (17), the time behaviour of the rate of star formation $\Psi(t)$ depends on the type of model in usage. In the closed-box description, the rate of star formation is maximum at the beginning, and since then it continuously decreases until galactic winds occur. In the infall model, owing to the competition between the rate of gas infall and gas consumption by star formation, the rate of star formation starts small, increases to a maximum and then declines. The age at which the peak occurs approximately corresponds to the infall time scale τ .

4.4. Galactic Winds

The models include the occurrence of galactic winds. When the energy deposit by the supernova explosions and stellar winds from massive stars (see below) exceeds the gravitational binding energy of the gas, the galactic wind is let occur halting further accretion and star formation, and ejecting all remaining gas. The mass of the luminous matter is frozen to the current value of the mass in stars. This is the real mass of the remnant visible galaxy to be used to compare theoretical results with observations. However, for the sake of simplicity we will always refer to the models by means of the asymptotic mass $M_L(T_G)$.

The galactic wind occurs when the total thermal energy of the gas equates the binding energy of the gas. The thermal energy of the gas is determined by the energy input from Type I and Type II supernovae and stellar winds ejected by massive stars (see also Theis et al. 1992).

The energy input from the three components are

$$E_{\text{th}}(t)_{\text{SNI}} = \int_0^t \epsilon_{\text{SN}}(t - t') R_{\text{SNI}}(t') M_L(T_G) dt' \quad (19)$$

$$E_{\text{th}}(t)_{\text{SNII}} = \int_0^t \epsilon_{\text{SN}}(t - t') R_{\text{SNII}}(t') M_L(T_G) dt' \quad (20)$$

$$E_{\text{th}}(t)_{\text{W}} = \int_0^t \epsilon_{\text{W}}(t - t') R_{\text{W}}(t') M_L(T_G) dt' \quad (21)$$

where R_{SNI} and R_{SNII} are the rates of supernova production, while R_{W} is the rate of gas ejection by massive stars in form of stellar winds. The time t' is either the explosion time or the time at which stellar winds occur.

To calculate $\epsilon_{\text{SN}}(t)$ and $\epsilon_{\text{W}}(t)$, the thermal content in the supernova remnant and stellar wind, respectively, we proceed as follows. The time variation of the supernova thermal content is taken from Cox (1972)

$$\epsilon_{\text{SN}}(t_{\text{SN}}) = 7.2 \times 10^{50} \epsilon_0 \text{ erg} \quad (22)$$

for $0 \leq t_{\text{SN}} \leq t_c$ and

$$\epsilon_{\text{SN}}(t_{\text{SN}}) = 2.2 \times 10^{50} \epsilon_0 (t_{\text{SN}}/t_c)^{-0.62} \text{ erg} \quad (23)$$

for $t_{\text{SN}} \geq t_c$, where ϵ_0 is the initial blast wave energy of the supernova in units of 10^{51} ergs, which is assumed equal to unity for all supernova types, $t_{\text{SN}} = t - t'$ is the time elapsed since the supernova explosion, and t_c is the cooling time of a supernova remnant, i.e.

$$t_c = 5.7 \times 10^4 \epsilon_0^{4/17} n_0^{-9/17} \text{ yr}, \quad (24)$$

where $n_0(t) = \rho_g(t)/m_H$ is the number density of the interstellar medium as a function of time, and $\rho_g(t)$ is the corresponding gas density.

The thermal content in the wind ejected by a massive star is estimated in the following way: a typical massive star (say in the range $20M_\odot$ to $120M_\odot$) in the course of its evolution ejects about half of the mass in form of a wind with terminal velocity of about 2000 km s^{-1} (see Chiosi & Maeder 1986) and, therefore, injects into the interstellar medium an energy of about

$$\epsilon_{W0} = \frac{1}{2} \left(\frac{M}{2} \right) V^2 \left(\frac{Z}{Z_*} \right)^{0.75} \text{ erg}, \quad (25)$$

where the term Z/Z_* takes into account a possible dependence on the metal content (cf. Kudritzki et al. 1987, Theis et al. 1992, and BCF for details).

Part of this energy will be radiated away and part will contribute to heat up the gas. In analogy with supernova remnants, we assume that this energy will cool down with the same law as for the energy injected by supernovae but with a different cooling time scale t_{cw} . This assumption stands on the notion that the energy content in the wind is continuously refueled by the radiative energy output from the emitting star. Therefore

$$\epsilon_W(t_W) = \epsilon_{W0} \text{ erg} \quad (26)$$

for $0 \leq t_W \leq t_{cw}$ and

$$\epsilon_W(t_W) = \epsilon_{W0} (t_W/t_{cw})^{-0.62} \text{ ergs} \quad (27)$$

for $t_W \geq t_{cw}$, where $t_W = t - t'$ is the time elapsed since the birth of a massive star, and t_{cw} is supposed to be of the same order of the evolutionary time scale of a massive star. Many preliminary calculations show that $t_{cw} = 15 \times 10^6 \text{ yr}$ is a good choice. It is easy to figure out that stellar winds can contribute by as much energy as classical supernova explosions and, therefore, they cannot be neglected in evaluating the total energy required to power galactic winds.

Other details on the calculation of $E_{\text{th}}(t)_{\text{SNI}}$, $E_{\text{th}}(t)_{\text{SNII}}$ and $E_{\text{th}}(t)_W$, the frequency of type I SN in particular can be found in BCF to whom we refer.

Suffice to remark that owing to the different metallicity distribution of infall models with respect to the closed box ones — it is indeed skewed towards the high metallicity end — the metallicity dependence of eq.(25) can be neglected. For the sake of consistency also the closed-box

models presented here are calculated with same assumption

The total thermal energy stored into the interstellar medium is

$$E_{\text{th}}(t) = E_{\text{th}}(t)_{\text{SNI}} + E_{\text{th}}(t)_{\text{SNII}} + E_{\text{th}}(t)_W. \quad (28)$$

Finally, a galactic wind is supposed to occur when

$$E_{\text{th}}(t) \geq \Omega_g(t). \quad (29)$$

This is an oversimplified description of the effect of the heating processes on triggering galactic winds. It implicitly assumes that the energy deposit is immediately homogenized in the gas, so that condition (29) is met at a certain age by the gas as a whole. In reality, the situation is much more complicated because cavities and tunnels of hot gas are likely to form (Matthews & Baker 1971), so that condition (29) can be met only locally and fractions of gas are ejected. This would imply that galactic winds rather than instantaneously take place over certain time scales that are difficult to evaluate at least in a simple model like this.

Furthermore, the deposit of thermal energy by supernova explosions and stellar winds, may also directly affect star formation. Indeed it is conceivable that as gas gets hotter and hotter, star formation gets less efficient as well.

Despite the above comments, all the results below are derived from models in which gas heating has no direct effect on star formation and galactic winds occur instantaneously when condition (29) is met by the gas as a whole.

Finally, the gas continuously ejected by dying stars is supposed to quickly heat up at high temperatures corresponding to the high velocity dispersion of the galaxy and not to be able to form new stars. The onset of galactic winds halts any star formation activity.

4.5. Model Parameters

Primary parameters of the models are:

1) The galactic mass $M_L(T_G)$. This is a mere label identifying the models. In the closed-box models it is the initial luminous mass of the galaxy, whereas in the infall models it represents the asymptotic value. In any case galactic winds lower the galactic mass to the value already stored in stars at the age of wind ejection. Models (closed-box and infall) are calculated for the following values of $M_L(T_G)$: $3 \times 10^{12} M_\odot$, $1 \times 10^{12} M_\odot$, $5 \times 10^{11} M_\odot$, $1 \times 10^{11} M_\odot$, $5 \times 10^{10} M_\odot$, and $1 \times 10^{10} M_\odot$. Thereinafter, all the models will be labelled by the mass $M_L(T_G)$ in units of $10^{12} M_\odot$ in turn shortly indicated by $M_{L,12}$.

2) The ratios R_L/R_D and M_L/M_D which fix the gravitational potential and the effect of dark matter. They have already been described in § 4.1

3) The exponent k and efficiency ν of the star formation rate. All the models are calculated assuming for $k = 1$. The parameter ν and associated time scale of stars

formation $t_{\text{SF}} = 1/\nu$ are varied in order to fit the major constraints of the problem.

4) The initial mass function (slope and ζ). The slope is kept constant, whereas ζ is let vary. We will show that $\zeta = 0.5$ is a good choice in order to get models with M/L_B ratios in agreement with the observational data (see below). This value is compatible with current prescriptions for chemical yields, indicating the range $0.3 < \zeta < 0.50$ (cf. Matteucci 1991, Rana 1991, and Trimble 1991).

5) The infall time scale τ . Although the time scale of mass accretion is considered as a free parameter of the models, we guess its value from the collapse time scale as function of $M_L(T_G)$. Assuming a homogenous distribution of matter in the volumes filled by the dark and luminous components, we can express the total mass density ρ_T as

$$\rho_T = (1 + \beta^2)\rho_L \quad (30)$$

where ρ_L can be determined with the aid of equation (10). Accordingly, the collapse time scale is (see also Arimoto & Yoshii 1987)

$$\tau(M_L(T_G)) = (1 + \beta^2)^{-0.5} \times 1.26 \times 10^8 \left(\frac{M_L(T_G)}{10^{12} M_\odot} \right)^{0.325} \text{ yr} \quad (31)$$

This relation yields the collapse time scales reported in Table 3 as function of the galactic mass. The time scale of mass accretion rules the infall process. For τ going to 0, the model reduces to an initial burst of star formation, while for τ stretching to ∞ , star formation does never stop. However, all the models below are calculated with $\tau = 0.1$ Gyr independently of the galactic mass. This choice reduces the number of parameters and appears fully appropriate to the present purposes.

6) The galaxy age T_G . This could be constrained to the model of the universe, i.e. to H_0 , q_0 , and red-shift of galaxy formation z_{for} . However, because of the uncertainty on the cosmological parameters, galaxy ages are let vary in the range of current estimates of the globular cluster ages, i.e. $13 \div 15 \pm 2$ Gyr (cf. Chiosi et al. 1992 for a recent review of the subject).

4.6. General remarks

Before concluding this section, we like to call the attention on three drawbacks of the models that might be used to invalidate the present analysis. The points in question are (i) the adoption of the one-zone description which does not allow us to take into account spatial gradients in colours and metallicity, (ii) the solar partition of abundances used in the stellar models, and finally (iii) our treatment of galactic winds.

(i) It is clear that the $(V-K)$ colours and magnitudes of the galaxies in the Bower et al. (1992a,b) sample refers to the whole galaxy, whereas the UV excess and its companion colour $(1550 - V)$ of Burstein et al. (1988) in most cases refer to the central region of a galaxy. The existence of gradients in colours and metallicities across elliptical galaxies is a well established observational fact (Carollo et al. 1993; Carollo & Danziger 1994, Davies et al. 1993, Schombert et al. 1993). This means that insisting on the one-zone description as in the present models, could be source of difficulty when comparing model results with observational data. It seems reasonable to argue that higher metallicities can be present in the central regions thus facilitating the formation of the right type of stellar sources of the UV radiation (H-HB and AGB manqué stars), whereas lower metallicities across the remaining parts of the galaxies would make the other integrated colours such as $(V-K)$ bluer than expected from straight use of the one-zone model for the whole galaxy.

(ii) Recent observations indicate that the pattern of abundances in elliptical galaxies is skewed towards an overabundance of α -elements with respect to Fe (cf. Carollo et al. 1993; Carollo & Danziger 1994). As already recalled, the library of stellar models in use is based on the standard (solar) pattern of abundances. Work is in progress to generate libraries of stellar models and isochrones with $[\alpha/\text{Fe}] > 0$. Preliminary calculations for the solar metallicity ($Z=0.02$) show the effect to be small in the theoretical CMD. In addition, calculations of the Mg_2 index from synthetic spectra for different metallicities and partitions of α -elements (Barbuy 1994) show that passing from $[\alpha/\text{Fe}] = 0.0$ to $[\alpha/\text{Fe}] = 0.3$ the Mg_2 index of an old SSP (15 Gyr) increases from 0.24 to 0.30.

(iii) Concerning galactic winds, we would like to comment on the recent claim by Gibson (1994) that using the above formulation for the energy deposited by supernova explosions and stellar wind, BCF underestimate the effect of supernova explosions and on the contrary overestimate the effect of stellar winds from massive stars. In brief, BCF assuming the CMR to be a mass-metallicity sequence looked at the metallicity that would generate the right colours. They found that considering supernovae as the only source of energy, by the time galactic winds occur, the gas fraction has become too low and the metallicity too high in turn, that the CMR is destroyed (it runs flat). To cope with this difficulty they included another

Table 3. *Free-Fall* time scale for the various masses

$M_{L,12}$	3	1	0.5	0.1	0.05	0.01
τ_{ff} (Gyr)	0.18	0.12	0.10	0.06	0.05	0.03

source of energy, i.e. the stellar winds from massive stars whose efficiency in powering galactic winds is described by equations (25) through (27) with t_{cw} as the key parameter for which the value of 1.5×10^7 yr has been adopted. This time roughly corresponds to the evolutionary lifetime of a $10 M_{\odot}$ star. In other words it is the time scale over which a group of newly formed O-type stars would evolve away from the SSP. They found that t_{cw} shorter than this value would not allow sufficient powering of the interstellar medium, so that galactic winds would occur much later than required by the CMR. Finally, BCF provided also an explanation for the different results found by other authors (Arimoto & Yoshii 1987, Matteucci & Tornambé 1987, Angeletti & Giannone 1990, and Padovani & Matteucci 1993). Admittedly, this additional source of energy was invoked to keep the standard interpretation of the CMR.

5. Closed-Box models of elliptical galaxies

In order to test the dependence of the results on the new library of SSPs we have re-calculated models of elliptical galaxies with the closed-box approximation. The guide line of the analysis is to search the combination of the parameters ν and ζ for which the most massive galactic model ($3M_{\text{L},12}$) at the canonical age of 15 Gyr matches the maximum observational values for (V-K) and (1550-V) colours, 3.5 and 2 respectively (cf. Figs.14 and 17 below). To this aim, assuming $k = 1$, different values of ν and ζ are explored.

In the closed-box approximation, ν simply fixes the time scale of star formation. The values under consideration are listed in Table 4. Furthermore, for each value of ν , six values of ζ are taken into account, i.e. $\zeta = 0.25, 0.30, 0.35, 0.40, 0.50$, and 0.60 . The analysis is limited to the case of the $3M_{\text{L},12}$ galaxy. The details of these models are not given here for the sake of brevity; they are available from the authors upon request. The results are shown in Fig. 6 which displays the correlation between (V-K) and (1550-V) and the corresponding observational data (shaded area). The (1550-V) colours are from Burstein et al. (1988), whereas the (V-K) colours are from Bower et al. (1992a,b).

Table 4. Adopted values for the parameter ν and associated time scale of star formation t_{SF}

ν (Gyr $^{-1}$)	20	15	10	5	1
t_{SF} (Gyr)	0.050	0.067	0.100	0.200	1.000

Clearly no combination of the parameters is found yielding models satisfying the above constraint (upper left corner of the shaded area in Fig. 6). Varying the age within the range allowed by the CMR (say 15 ± 2 Gyr) does not help to match both colours of the reference galactic model. Similar results are obtained for the other galactic masses. There is a tight relationship between the theoretical (1550-V) and (V-K) which can be easily understood in terms of intrinsic behaviour of the closed-box model and the dependence of the two colours on the metallicity. As shown by BCF, the maximum metallicity determines the UV intensity and hence (1550-V) colour, whereas the mean metallicity governs the (V-K) colour.

Fig. 6. The (1550-V) versus (V-K) relationship for closed-box models. The shaded area shows the observational data. The models are calculated for different values of ζ as indicated, and for all the values of ν listed in Table 4. The solid line shows models with $\zeta = 0.40$ and the same values of ν as before but in which the low-metallicity component is taken away. All the models refer to the $3M_{\text{L},12}$ galaxy

In a closed-box system, the current (maximum) metallicity obeys the relation:

$$Z(t) = Y_z \ln \mu^{-1} \quad (32)$$

where $\mu = M_g(t)/M_L(T_G)$ is the fractionary mass gas and Y_z is the chemical yield per stellar generation. This relation holds for $Z \ll 1$. The mean metallicity is given by:

$$\langle Z(t) \rangle = \frac{\int \Psi(t) Z(t) dt}{\int \Psi(t) dt} \quad (33)$$

With the aid of eqs. (32), (33) and (17) we get the relationship between $\langle Z(t) \rangle$ and $Z(t)$ shown in Fig. 7. Owing to the low-metal skewed distribution typical of the closed-box models, if the maximum metallicity rises to values at which the H-HB and AGB manqué stars are formed and in turn the dominant source of the UV radiation is switched on (cf. BCF for all details), the mean metallicity is too low to generate the right (V-K) colours. In order to prove this statement, in Fig. 6 we show models in which all the stars with $Z \leq 0.008$ are artificially removed (solid line). As expected, solutions are now possible. On the one hand this result confirms the conclusions by BCF about the intrinsic difficulty of the closed-box models, on the other hand it makes evident that the success or failure of a particular spectro-photometric model in matching the observational data depends very much on details of the adopted spectral library. With the one used by BCF reasonable match of the data was possible even with the closed-box scheme, but for the before mentioned marginal discrepancy of the ISED in the region 2000 Å to 3500 Å. With the new library this is no longer feasible.

Fig. 7. The $Z(t)$ versus $\langle Z(t) \rangle$ for the same models as in Fig. 6. Note the linear relationship between the two metallicities for models with the same ζ . See the text for more details

6. Infall models of elliptical galaxies

In order to check whether infall models can cope with the above difficulty, we perform a preliminary analysis of the problem calculating infall models with the same parameters ν and ζ as for the closed-box case. In these models

$k = 1$, $\tau = 0.1$ Gyr, and the galactic mass is $3M_{L,12}$. The results are shown in Fig. 8. With the infall scheme many models exist whose (V-K) and (1550-V) match the observational data.

Fig. 8. The (1550-V) versus (V-K) for all infall models. The shaded area indicates the range spanned by the observational data. The models are calculated for different values of ζ as indicated, and for all the values of ν listed in Table 4. All the models refer to the $3M_{L,12}$ galaxy

The reason of the success is due to the law of chemical enrichment of infall models (cf. Tinsley 1980b)

$$Z(t) = Y_z \left[\ln\left(\frac{1}{\mu}\right) - 1 \right] \quad (34)$$

where all the symbols have the same meaning as in eq. (32), which leads to the relationship between the maximum and mean metallicity shown in Fig. 9. Since the metallicity distribution of infall models is skewed towards the high metallicity side, at given maximum metallicity higher mean metallicities are found that allow us to match of the observational (V-K) and (1550-V) colours at the same time. The details of these models are not given here for the sake of brevity. They are available upon request.

7. Properties of infall models

Not all the models presented in the previous section are equally acceptable because other important constraints of the problem have not yet been taken into account. These are the slope and mean colours of the CMR for elliptical galaxies, the mass to blue luminosity ratio M/L_B , the

Fig. 9. The $Z(t)$ against $\langle Z(t) \rangle$ for the open models as in Fig. 8. Note the linear relationship between the two metallicities for models with the same ζ . See the text for more details

overall fit of the UV excess, i.e. colour (1550–V), shape of the ISED, and Mg_2 versus (1550–V) relation.

It turns out that the ratio M/L_B requires $\zeta = 0.5$, whereas the combined effect of all the remaining constraints confines ν in the range $1 < \nu < 12$. More precisely, from $\nu = 12$ for the $3 M_{L,12}$ galaxy to $\nu = 1$ for the $0.01 M_{L,12}$ object. The various points will be examined in more detail below.

The main properties of the models in question are given in Table 5. This consists of two parts. The first one contains the key quantities characterizing the models at the stage of wind ejection: columns (1), (2) and (3) are the parameters ν , ζ , and $M_L(T_G)$ identifying the model, respectively; column (4) is the age in Gyr at which the galactic wind occurs; columns (5) and (6) are the fractionary mass of gas $G(t)$ and living stars $S(t)$ both in units of $M_L(T_G)$; columns (7) and (8) are the maximum and mean metallicity, respectively; column (9) is the rate of star formation $\Psi(t)$ (in M_\odot/yr); finally columns (10) through (14) are the binding energy of the gas (Ω_g), the total thermal energy of the gas (E_g), and the contribution to it by type I supernovae, type II supernovae, and stellar winds, respectively. All energies are in units of 10^{50} ergs. The second part of Table 5 presents the integrated magnitudes and colours of the model galaxies at five different ages. Columns (1), (2) and (3) identify the model by means of ν , ζ , and $M_L(T_G)$, respectively; column (4) is the age in Gyr, columns (5) and (6) are the integrated absolute bolometric (M_{bol}) and visual magnitude (M_V); fi-

nally, columns (7) through (11) are the integrated colours (U–B), (B–V), (V–R), (V–K) and (1550–V), respectively. We remind the reader that all the integrated magnitudes refer to the current amount of the galaxy mass in form of living stars (see below for more details).

7.1. Chemical Structure

The time variation of the fractionary gas content $G(t)$ and metallicity $Z(t)$ are shown in Fig. 10, whereas that of the star formation rate (in units of M_\odot/yr), thermal (E_{th}) and binding energy of the gas $\Omega_g(t)$ (both in units of 10^{50} erg) are displayed in Fig. 11.

As expected, the rate of star formation (Panel a of Fig. 11) starts very small, grows to a maximum, and were it not for the onset of galactic wind and consequent interruption of the stellar activity, it would decline again. The initial period of very low activity is the reason why infall models avoid the so called G-Dwarf problem.

The metallicity distribution among the stars of the model galaxies of Table 5 is given in Figs. 12 and 13. In the former, we show the relative total mass dM in stars per metallicity bin. This is normalized to $M_L(T_G)$. For the purposes of comparison we present also one case of closed-box models (the $3M_{L,12}$ galaxy: thick line).

The metallicity distribution in galaxies of different mass is shown in Fig. 13 displaying the cumulative fractionary mass in alive stars as a function of Z . In this case the distribution is normalized to the total mass in alive stars at the age of 15 Gyr. We notice that while for the most massive galaxy only 20% of the stars have a metallicity below solar, this percentage increases at decreasing galaxy mass. Furthermore, the maximum metallicity decreases at decreasing galaxy mass. Indeed, galaxies less massive than $1M_{L,12}$ have only stars with $Z < Z_\odot$.

7.2. Galactic winds

The onset of galactic winds occurs within the first 0.5 Gyr for all the masses under consideration (cf. the entries of Table 5). In contrast to previous models of elliptical galaxies with galactic winds, in which the onset of these is found to occur later in more massive objects (cf. BCF and references therein), in these models the wind occurs earlier in more massive galaxies than in the low mass ones. This can be understood as the result of the efficiency of star formation per unit mass of gas (ν) increasing from $\nu = 1$ to $\nu = 12$ as the galactic mass goes from 0.01 to $3M_{L,12}$. This trend is imposed by the simultaneous fit of the slope and mean colours of the CMR and the dependence of the UV excess on the galaxy luminosity and hence mass (see below).

The result agrees with the suggestion by Matteucci (1994) to explain the high value of the $[Mg/Fe]$ observed in the brightest elliptical galaxies and its decrease toward the solar value at decreasing luminosity of the galaxy.

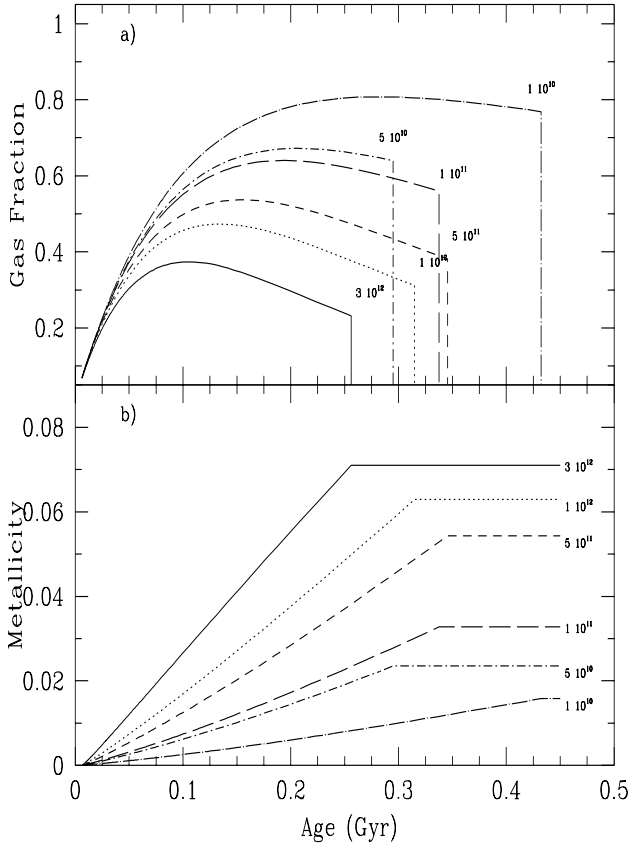


Fig. 10. The gas fraction $G(t)$ (Panel a) and metallicity $Z(t)$ (Panel b) as a function of the age in Gyr for the model galaxies with $\zeta = 0.50$, ν increasing with the mass, and galactic mass from $3 M_{L,12}$ to $0.01 M_{L,12}$. In Panel (a), the intersection of the curves with the vertical lines indicates the stage of the onset of galactic winds and consequent drop-off of the gas content. In Panel (b) the horizontal lines show the constant metallicity after the interruption of star formation by galactic winds

Finally, we like to remark that owing to the onset of galactic winds and subsequent interruption of the star formation activity, the remnant galaxy made of stars has a mass which is only a fraction of its nominal value. The real current masses of the galaxies at the stage of the galactic wind are given in Table 6. This contains the asymptotic mass M_L (column 1), the age at onset of the galactic wind (column 2), the sum of the star and gas mass in units of $M_{L,12}$ (column 3), and finally the mass in stars (column 4) in the same units.

7.3. Colour-magnitude relation

The CMR for the models of Table 5 is compared with the observational one in Fig. 14. The theoretical CMR is given for several values of the age in the range 5 to 17 Gyr. The data are from Bower et al. (1992a,b): open circles are the

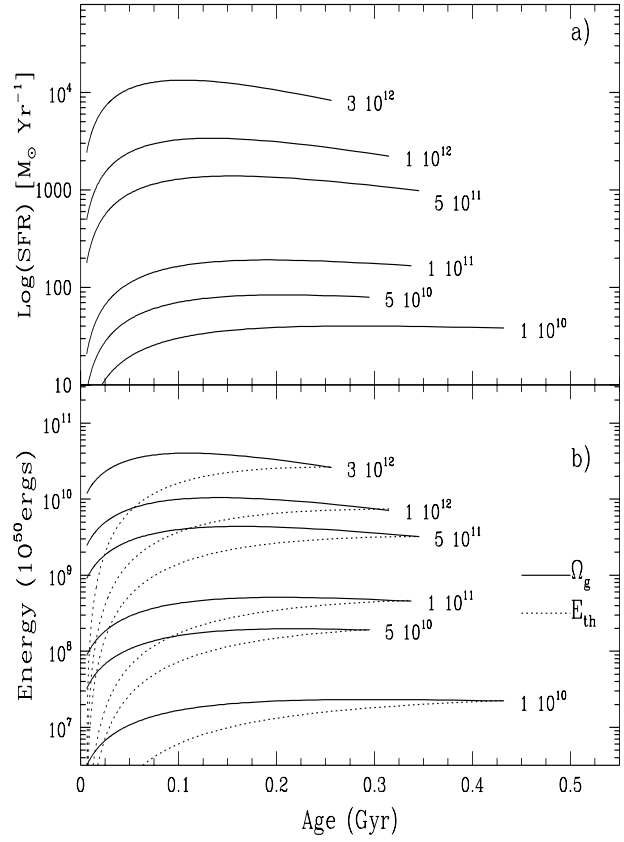


Fig. 11. The same as in Fig. 10 but for star formation rate $\Psi(t)$ in units of $M_{\odot} \text{yr}^{-1}$ (Panel (a)) and the gravitational binding energy $\Omega_g(t)$ and the thermal content of the gas $E_{th}(t)$, both in units of 10^{50} erg (Panel (b))

galaxies in Virgo, while the filled circles are the galaxies in Coma. The absolute magnitudes V are calculated assuming for Virgo the distance modulus $(m - M)_0 = 31.54$ (Branch & Tammann 1992) and applying to the galaxies in Coma the shift $\delta(m - M)_0 = 3.65$ (Bower et al. 1992a,b). As expected the theoretical CMR nicely fit both the slope and the mean colours of the observational CMR.

7.4. Mass to blue luminosity ratio

The mass to blue luminosity ratio M/L_B is found to be very sensitive to the IMF, and at given slope to ζ . The observational M/L_B ratios (in solar units) of Bender et al. (1992, 1993) and Terlevich & Boyle (1993) — scaled to the Hubble constant $H_0 = 50 \text{ km sec}^{-1} \text{ Mpc}^{-1}$ — are in the range 1 to 18. With the adopted IMF (eq. 17) the mean value of the observational data is matched adopting $\zeta = 0.50$. The theoretical M/L_B ratios for the models of Table 5 are given in Table 7, which lists the age in Gyr in column (1), $M_L(T_G)$ in column (2), the blue magnitude M_B in column (3), $(B-V)$ colour in column (4), the

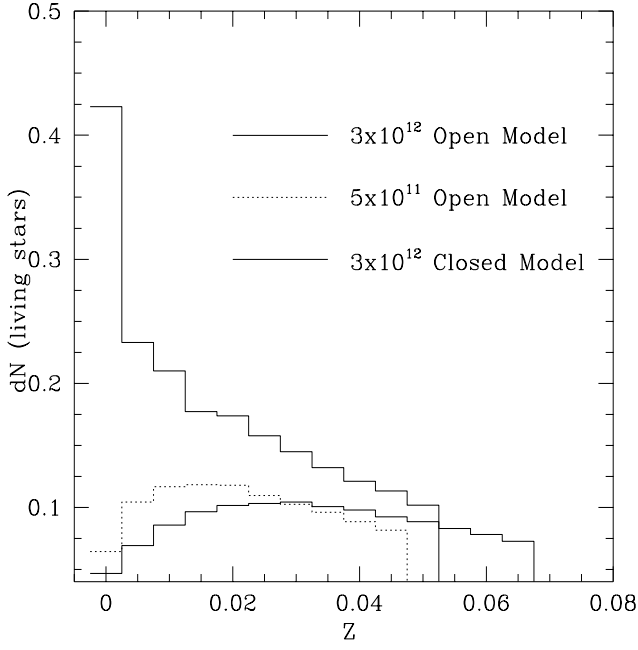


Fig. 12. The relative number of alive stars per metallicity bin normalized to $M_L(T_G)$. The solid and dotted lines refer to infall models with $3M_{L,12}$ and $\nu = 12$, and $0.5 M_{L,12}$ and $\nu = 5.2$, respectively. Both are calculated with $\zeta = 0.50$. The thick line displays the closed-box model with $3M_{L,12}$, $\nu = 20$, and $\zeta = 0.40$

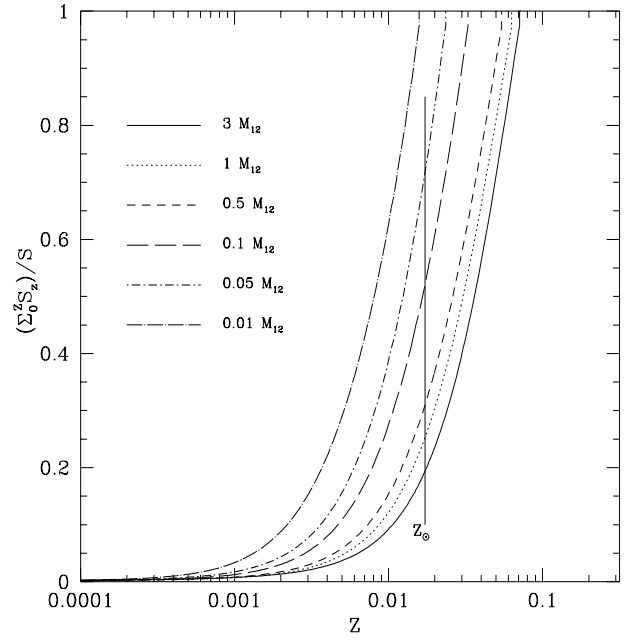


Fig. 13. The cumulative fractionary mass of alive stars as function of the metallicity for the model galaxies with mass equal to 3, 1, 0.5, 0.1, 0.05, and 0.01 $M_{L,12}$, $k = 1$, $\zeta = 0.50$, and ν varying with the galactic mass. The normalization mass is the present-day value of the total mass in alive stars (see the data of Table 5)

Table 6. The mass of gas and stars at the onset of galactic winds for models with different mass. The age t_{gw} at which the galactic wind occurs is in Gyr. Masses are in units of $M_{L,12}$.

$M_L(T_{GAL})$	t_{gw}	$M_L(T)S(t) + M_L(T)G(t)$	M_{TOT}
3	0.26	2.088 ± 0.696	2.784
1	0.31	0.648 ± 0.312	0.960
0.5	0.35	0.295 ± 0.191	0.485
0.1	0.34	0.041 ± 0.056	0.097
0.05	0.29	0.016 ± 0.032	0.048
0.01	0.43	0.002 ± 0.008	0.010

blue-luminosity L_B in column (5), and the mass to blue luminosity ratio M/L_B in column (6). The comparison with the observational data is presented in Fig. 15 for different values of the age. Although a certain spread among the ages of galaxies cannot be excluded, the theoretical M/L_B versus M_B relationship seems to be flatter than the mean slope traced by the observational data. The analysis of the problem shows that in order to reconcile theory with observation either a variation of the IMF slope or the frac-

tion ζ with the galactic mass or both should be required (cf. Renzini & Ciotti 1993).

7.5. On the nature of the UV excess

Key features of the UV excess (Burstein et al. 1988) to be interpreted by the galactic models are:

- The correlation of the $(1550 - V)$ colour with the index Mg_2 , the velocity dispersion Σ , and the luminosity (mass) of the galaxy.
- The drop-off of the UV flux short-ward of about 1000 \AA observed in the nucleus of M31 by Ferguson et al. (1991) and Ferguson & Davidsen (1993) which requires that the temperature of the emitting source must be about 25,000 K. Only a small percentage of the $912 \leq \lambda \leq 1200 \text{ \AA}$ flux can be coming from stars hotter than 30,000 K and cooler than 20,000 K.

Excluding ongoing star formation, the UV excess owes its origin to an old component that gets hot enough to power the integrated spectral energy distribution (ISED) of a galaxy in the far UV regions. Three candidates are possible each of which likely contribute to the total emission in proportions that depend on the particular history of star formation of the galaxy under consideration (cf. Greggio & Renzini 1990, BCF)

Fig. 14. The CMR for model galaxies with mass of 3, 1, 0.5, 0.1, 0.05, and 0.01 $M_{L,12}$ and the same set of parameters as in Fig. 13. The star formation rate is characterized by $k = 1$. As indicated CMRs for different ages are plotted. The data are for the galaxies in Virgo (*open circles*) and Coma (*filled circles*) by Bower et al. (1992a,b). The typical uncertainty in the photometric data is shown by the vertical bars

- The classical post asymptotic giant branch (P-AGB) stars (see Bruzual 1992, Bruzual & Charlot 1993, Charlot & Bruzual 1991). However, even if a small drop-off can be predicted just long-ward of 912 Å, they cannot be the sole source of UV flux because of their high mean temperature (about 100,000 K) and weak dependence on the metallicity. Nevertheless, these stars have been detected with HST observations in the nucleus of M31 and can contribute by as much as 50% to the UV light (Bertola et al. 1995).
- Very blue horizontal branch (HB) stars of extremely low metallicity (Lee 1994). These stars have effective temperatures hotter than about 15,000 K but much cooler than those of the P-AGB stars. Therefore, depending on their actual effective temperature, they can generate ISEDs in agreement with the observational data. However, most likely they are not the dominant source of the UV flux because BCF showed that in the wavelength interval $2000 < \lambda < 3000$ Å the ISEDs of the bulge of M31 and of elliptical galaxies like NGC 4649 are fully consistent with the notion that virtually no stars with metallicity lower than $Z=0.008$ exist in the mix of stellar populations.
- Finally, the hot horizontal branch (H-HB) and AGB-manqué stars of very high metallicity (say $Z > 0.07$)

Fig. 15. The logarithm of the mass to B-luminosity ratio M/L_B versus the absolute blue magnitude M_B for models with $k = 1$, ν increasing with the galactic mass, and $\zeta = 0.50$. The mass used to calculate M/L_B and M_B refers to the present-day mass in the form of alive stars. The ratio M/L_B is expressed in solar units. The displayed quantities refer to ages from 17 to 5 Gyr. The dashed line is the relation by Terlevich & Boyle (1993) for $H_0 = 50 \text{Kms}^{-1} \text{Mpc}^{-1}$. The data are by Bender et al. (1992, 1993), i.e. open dots: giant elliptical's; full dots: intermediate elliptical's; stars: bright dwarf elliptical's; open squares: compact elliptical's; open triangle: bulges

which are expected to be present albeit in small percentages in the stellar content of bulges and elliptical galaxies in general. Indeed, these stars have effective temperatures in the right interval and generate ISEDs whose intensity drops short-ward of about 1000 Å by the amount indicated by the observational data (Ferguson et al. 1991, Ferguson & Davidsen 1993).

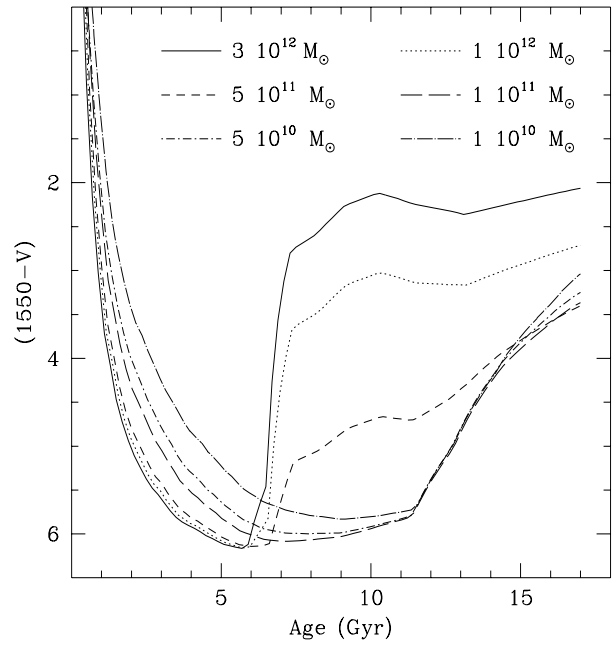
The appearance of the various types of UV sources is governed by several important physical factors, each of which is affected by a certain degree of uncertainty still far from being fully assessed. These are the efficiency of mass loss during the RGB and AGB phases, in particular whether or not it contains a strong dependence on the metallicity, the enrichment law $\Delta Y / \Delta Z$ fixing the correspondence between helium and metal contents of the stellar models, and finally for the specific case of P-AGB stars the detailed relation between the initial and final mass of the stars at the end of the AGB phase. It is beyond the scope of this paper to examine the above uncertainties in detail. They have amply been discussed by Greggio & Ren-

Table 7. The mass to blue-luminosity ratio (in solar units) as function of the age for the model galaxies with different mass.

Age	$M_L(T_G)$	M_B	$(B-V)$	$\frac{L_B}{L_\odot}$	$\frac{M}{L_B}$
17	3.00	-22.70	0.998	1.867e11	6.844
17	1.00	-21.50	1.000	6.200e10	6.516
17	0.50	-20.70	0.995	2.970e10	6.195
17	0.10	-18.73	0.948	4.808e9	5.241
17	0.05	-17.77	0.916	2.003e9	4.719
17	0.01	-15.85	0.861	3.398e8	4.032
15	3.00	-22.78	1.001	2.008e11	6.364
15	1.00	-21.58	1.002	6.699e10	6.031
15	0.50	-20.79	0.998	3.218e10	5.718
15	0.10	-18.82	0.955	5.238e9	4.811
15	0.05	-17.87	0.928	2.180e9	4.335
15	0.01	-15.94	0.880	3.712e8	3.691
12	3.00	-22.97	0.981	2.397e11	5.333
12	1.00	-21.78	0.985	8.009e10	5.044
12	0.50	-20.98	0.983	3.855e10	4.773
12	0.10	-19.02	0.946	6.310e9	3.994
12	0.05	-18.07	0.922	2.623e9	3.603
12	0.01	-16.14	0.880	4.442e8	3.084
10	3.00	-23.18	0.967	2.903e11	4.403
10	1.00	-21.98	0.973	9.612e10	4.203
10	0.50	-21.18	0.971	4.600e10	4.000
10	0.10	-19.20	0.932	7.447e9	3.384
10	0.05	-18.24	0.908	3.087e9	3.061
10	0.01	-16.31	0.868	5.214e8	2.627
8	3.00	-23.41	0.936	3.607e11	3.543
8	1.00	-22.21	0.946	1.188e11	3.401
8	0.50	-21.40	0.946	5.665e10	3.248
8	0.10	-19.43	0.909	9.171e9	2.748
8	0.05	-18.47	0.887	3.809e9	2.481
8	0.01	-16.55	0.850	6.468e8	2.118
5	3.00	-23.87	0.910	5.475e11	2.334
5	1.00	-22.68	0.908	1.830e11	2.208
5	0.50	-21.88	0.902	8.790e10	2.093
5	0.10	-19.89	0.862	1.407e9	1.791
5	0.05	-18.92	0.837	5.754e9	1.642
5	0.01	-16.98	0.792	9.656e8	1.419

zini (1990) and BCF to whom we refer. Suffice to recall that

- P-AGB stars are always present in the stellar mix of a galaxy. The major difficulty with these stars is their high effective temperature, and the precise relation between their mass and that of the progenitor (and hence the turn-off mass and age). The response of the UV flux to details of initial-final mass relation (for instance its dependence on the metallicity) is so strong that firm conclusions cannot yet be reached. For instance at ages older than about 10 Gyr, the whole problem is driven by the initial-final mass relation in the mass range $0.8 \div 1.0 M_\odot$.
- H-HB and AGB-manqué are thought to be typical of low mass stars with metallicity $Z \gg Z_\odot$. Their formation can be obtained either with low values of the en-

**Fig. 16.** The colour (1550-V) as function of the age for galaxies of different $M_{L,12}$ and mean and maximum metallicity. These latter increase with the galactic mass. Note the gradual transition going from the $3M_{L,12}$ galaxy, in which H-HB and AGB-manqué stars dominate the UV flux, to the $0.01 M_{L,12}$ galaxy, in which only the P-AGB stars contribute to it

richment ratio ($\Delta Y/\Delta Z \simeq 1$) and strong dependences of the mass-loss rates on the metallicity (Greggio & Renzini 1990) or even with canonical mass-loss rates and suitable enrichment laws ($\Delta Y/\Delta Z \simeq 2.5$) as in Horch et al. (1992) and Fagotto et al. (1994a,b,c).

The present spectro-photometric models owe their UV flux to the combined effect of P-AGB stars and H-HB and AGB-manqué objects, these latter being very sensitive to the metallicity distribution. The different nature of the UV source at varying galactic mass and mean and maximum metallicity in turn is best illustrated by the age-(1550-V) colour relation shown in Fig. 16. In the most massive objects the UV flux is dominated by the H-HB and AGB-manqué stars (uprise in the age range 5.6 to 6.8 Gyr), whereas in the less massive galaxies the UV excess is entirely produced by the P-AGB stars (gradual uprise starting from 11.5 Gyr).

7.6. The Mg_2 index

The correlation between the colour (1550-V) and the Mg_2 index is shown in Fig. 17 together with the observational data of Burstein et al. (1988). The index Mg_2 is derived from the broad band colour (V-K) using the calibration of Buzzoni et al. (1992), which fits the data for elliptical galaxies by Davies et al. (1993) and Frogel et al. (1978)

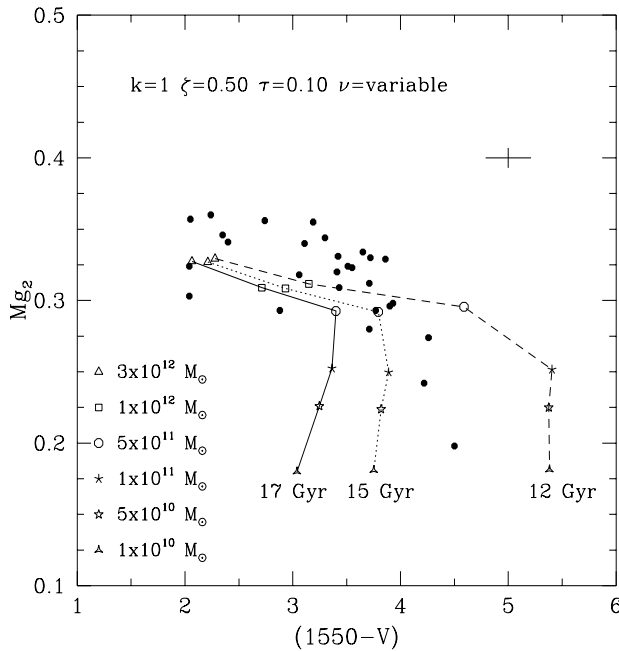


Fig. 17. Comparison of the theoretical relation Mg_2 versus $(1550-V)$ relation with the data by Burstein et al. (1988) indicated by the filled circles. The theoretical Mg_2 is obtained from the $(V-K)$ colour according to the analytical fit due to Buzzoni et al. (1992): $Mg_2 = 0.24(V - K) - 0.49$. The effect of the age is brought into evidence by drawing with different symbols the Mg_2 – $(1550-V)$ relation for three different values of the age, i.e. 12, 15, and 17 Gyr. Along the three curves (dashed, dotted and solid, respectively, the galaxy mass and maximum metallicity decrease from left to right. The data are from Table 5. The cross shows the typical error bars of the data. See the text for more details

and is also consistent with those between $(V-K)$ and central velocity dispersion ($\text{Log}\Sigma_0$) by Bower et al. (1992a,b) and between Mg_2 and $\text{Log}\Sigma_0$ by Bender et al. (1992, 1993). This choice is imposed by the lack of sufficient resolution in the library of stellar spectra that does not allow us to apply the standard definition of this narrow band feature (Faber et al. 1977). Detailed calculations of line strength indices according to the Worthey et al. (1994) calibrations are presented in Bressan et al. (1995) to whom we refer. In spite of this limitation, the Mg_2 versus $(1550-V)$ relationship of Fig. 17 is fully adequate to the present purposes. As expected the Mg_2 versus $(1550-V)$ relation depends both on the age and metallicity via the galactic mass thus partly explaining the scatter in the observational data. We notice in particular that at given age the Mg_2 index decreases at decreasing galactic mass (mean and maximum metallicity in turn). There is a marginal discrepancy in the theoretical Mg_2 indices that are somewhat smaller than the observational values. This can be attributed to the effect of the α -element partition discussed in section 4.6.

Correcting for it would likely increase the theoretical Mg_2 by 0.05 thus bringing the theoretical prediction to agree with the observational data.

7.7. Detailed comparison of ISEDs

The theoretical ISEDs reasonably match the observational ones both in the far UV and all over a large range of wavelength from the UV to the near infrared. To illustrate the first point we show how our models match the observed ultraviolet ISED of two prototype galaxies: NGC 4649 a strong source with $(1550-V)=2.24$ and NGC 1404 an intermediate source with $(1550-V)=3.30$. The former is best matched by the model with $3M_{L,12}$ and age of 15 Gyr, whereas the latter is reasonably reproduced by the model with $1M_{L,12}$ and same age. The comparison is shown in the two panels of Fig. 18. Firstly, we notice that there is no excess of flux in the range 2000 - 3500 Å as it occurred with the closed-box approximation (see BCF). As expected, the infall models are able to solve the analog of the G-Dwarf problem in the ISED of elliptical galaxies. Secondly, the source of UV flux gets more and more weighted toward the H-HB and AGB manqué channel as compared to the classical P-AGB stars at increasing galaxy mass and hence maximum attainable metallicity. The trend can be inferred from the decreasing flux intensity at about 1000 Å with respect to that at shorter wavelengths passing from a massive to a less massive galaxy, and also from the relative value of the flux in the region 1000 - 2000 Å to that in the visual (compare top and bottom panels of Fig. 18). Furthermore, the theoretical ISEDs have the kind of fall-off at about 1000 Å indicated by the observations of Ferguson et al. (1991) and Ferguson & Davidsen (1993) in elliptical galaxies with UV excess. Finally, the two model galaxies have $(1550-V)$ colours that fairly agree with the observational data: 2.21 for the most massive galaxy and 2.93 for the less massive one (see the data in Table 5).

Concerning the second point, we compare the ISED of NGC 4649 from 1000 to 11,000 Å (from the far UV to the near infrared) with the theoretical ISED of the $3M_{L,12}$ model. The comparison is shown in Fig. 19. Mounting of the theoretical ISED on the observational one is made imposing coincidence at about 5500 Å. In general the agreement is satisfactory. However there are a few points of discrepancy worth being noticed. Indeed, there is a deficiency of flux in the theoretical ISED above 7500 Å and some scatter in the UV region as indicated by the residuals shown in panel b of Fig. 19.

7.8. UV-excess as age probe

In this section, we discuss the possibility of dating galaxies by means of the UV-excess. BCF have shown that signatures in the colour evolution (like those caused by the appearance of AGB stars) manifest themselves at early epochs cannot be used as age probes because their detec-

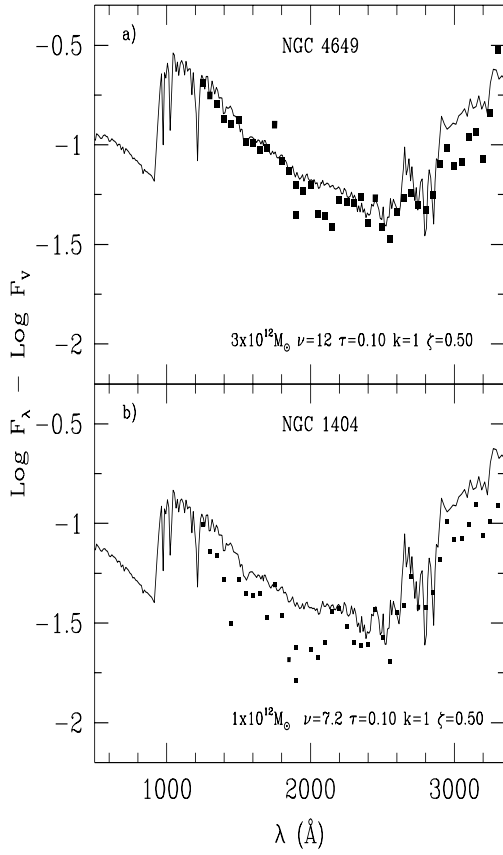


Fig. 18. Panel (a): comparison of the spectrum of NGC 4649 (filled squares) with the theoretical ISSED of the model with mass $3M_{L,12}$ (solid line). The observational ISSED is from Burstein et al. (1988). Note the remarkable agreement with the data. **Panel (b):** the same as in Panel (a) but for the galaxy NGC 1404 (filled squares) and the theoretical ISSED of the model with mass $1M_{L,12}$.

tion as a function of the red-shift is wiped out by cosmological effects. On the contrary, the onset of the UV-excess caused by the old, high metallicity stars is a very promising candidate. The most favourable object to look at is a massive (luminous) object with strong UV-excess, such as our model with $3M_{L,12}$.

To illustrate the point in Fig. 20 we show the evolution of the colours, (U-B), (B-V), (V-K) and (1550-V) as a function of the age for the $3M_{L,12}$ model.

Following the initial period of stellar activity (in this galaxy confined within the first 0.26 Gyr), no sign of evolution is visible in the colours (U-B) and (B-V) which get redder and redder at increasing age. The colour (V-K) has a marked drop-off at the age at which the first AGB stars occur (a few 10^8 yr) and remains almost constant afterward. The very young age at which the drop-off occurs is the cause of the failure of the (V-K) colour as age indicator. As a matter of facts, this young age would

Fig. 19. Panel (a): the observed spectrum of the elliptical galaxy NGC 4649 indicated by open squares (Lucio Buson, 1993, private communication). The solid line shows the theoretical ISSED for the model with $3M_{L,12}$, $k=1$, $\nu=12.0$, $\zeta=0.50$, $\tau=0.10$ Gyr, and age of 15 Gyr. Note the good agreement. **Panel (b):** residuals (open circle) between the theoretical ISSED and the data.

correspond to high values of the red-shift thus rendering detection difficult and cosmological distortion of the ISSED and hence colour very large.

The colour (1550-V) is by far more suited. First, following the interruption of the star formation activity by galactic winds, its colour drops to very “red values” (low UV flux). Subsequently, at much older ages in coincidence with the appearance of the old stars emitting UV radiation (P-AGB and above all H-HB and AGB-manqué objects) it becomes “blue” again (see Fig. 16). For our test galaxy the uprise in the (1550-V) colour occurs at the age of about 5.6 Gyr to which a relatively low value of the red-shift corresponds.

It goes without saying that the age in question depends the adopted $\Delta Y/\Delta Z$ and efficiency of mass loss during the RGB and AGB phases. The explanation of the UV-excess in elliptical galaxies imposes some constraints both on $\Delta Y/\Delta Z$ and mass loss. Our choices for both constitute

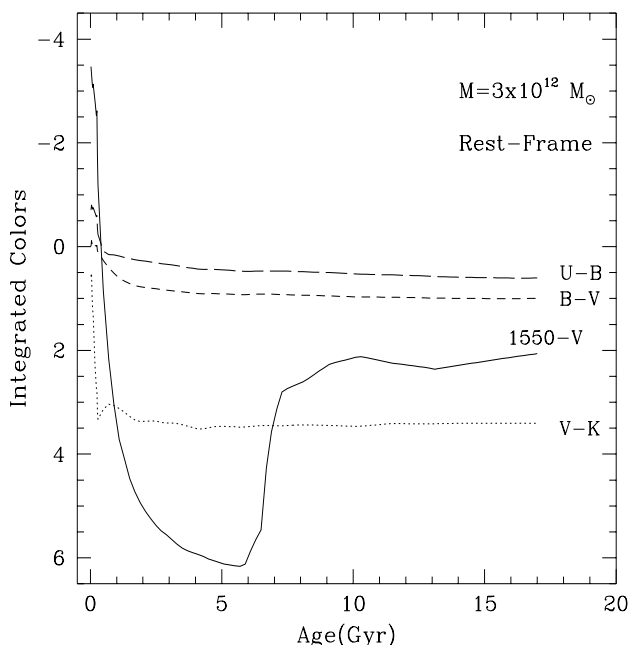


Fig. 20. The integrated colours (1550-V), (U-B), (B-V) and (V-K) as a function of the rest frame age for the model with $3 M_{L,12}$, $k = 1$, $\nu = 12.0$, $\zeta = 0.50$ and $\tau = 0.10$ Gyr

a sort of lower limit, and therefore the corresponding age of the UV-upturn is a sort of upper limit. However, much higher $\Delta Y/\Delta Z$ and mass loss rates are not very likely.

It follows from this analysis that not only the UV-excess is a powerful probe of galaxy ages but the detection of its onset at a certain red-shift together with the measurements of its fall off as a function of the red-shift would allow us to establish useful relations between H_0 , q_0 and z_{for} . Future observations will certainly make feasible the detection of this important evolutionary effect.

8. Summary and conclusions

In this paper we have presented one zone chemo-spectrophotometric models of elliptical galaxies with infall of primordial gas. Galaxies are supposed to be made of two components, i.e. luminous and dark matter. While the mass of the dark component is assumed to be constant with time, that of the luminous material is supposed to fall at a suitable rate into the common potential well.

The main motivation for this type of model was to mimic the collapse of a galaxy and to cope with the difficulty reported by BCF using the closed-box scheme, i.e. the analog of the G-Dwarf problem. The adoption of the infall scheme adds another dimension to the problem, i.e. the time scale of mass accretion τ . Taking the free-fall time scale as a reference, instead of changing τ with the galaxy mass, low mass galaxies would have got closer and closer to the closed-box approximation, we prefer to adopt

the unique value $\tau = 0.1$ Gyr, i.e. the free-fall time scale for a typical galaxy with mass $0.5 M_{L,12}$.

The models also include the occurrence of galactic winds that have long been considered the key physical process governing the CMR of elliptical galaxies. The galactic winds are supposed to occur when the energy input from supernovae and stellar winds from luminous early type stars equals the gravitational binding energy of the gas. It goes without saying that this is a point of great uncertainty of the models. In this respect our approach does not go beyond other current models of elliptical galaxies with galactic winds taken into account. Both the rate of supernova explosions and cooling of the energy injected by these stars are treated in the standard fashion (see for instance Arimoto & Yoshii 1987, Matteucci & Tornambé 1987, Brocato et al. 1990, Angeletti & Giannone 1990). However, in agreement with BCF and in contrast with other authors, we confirm that if the CMR of elliptical galaxies has to be understood a mass-metallicity sequence of nearly coeval objects, in addition to supernova explosions another source of energy must be at work in order to trigger galactic winds before the metallicity has grown to such high values that only very red colours are possible.

The adoption of the infall scheme has the advantage over the closed-box description that with the law of star formation proportional to $M_g^k(t)$, the rate of star formation as a function of time starts small, grows to a maximum and then declines thus easily avoiding the excess of zero metal stars typical of the closed-box scheme. Indeed, infall models have the metallicity distribution of its stellar content skewed towards relatively high metallicities.

As repeatedly said, the bottom line to contrive the various parameters of the models has been the simultaneous fit of many properties of elliptical galaxies. We have found that with the new library of stellar spectra in usage the simultaneous fit of the (V-K) and (1550-V) colours is not possible with the closed-box description, whereas this is feasible with the infall scheme. The fit of the slope and mean colours of the CMR and UV excess of elliptical galaxies required that the efficiency of star formation per unit mass of gas (ν) must increase with the galaxy mass. As a consequence of this, the overall duration of the star forming activity (before the onset of galactic winds) in massive galaxies is shorter than in the low mass ones. This kind of trend is in agreement with the hint coming from the observational dependence of the [Mg/Fe] ratio with the galaxy luminosity (and hence mass) and the suggestion based on chemical models advanced by Matteucci (1994).

As far as the simultaneous fit of the CMR, (V-K) versus V, and the (1550-V) versus M_{g2} relation by our model galaxies as a whole imply that the two observational sets of data refer to the same region of the galaxies. While the data on the UV-excess, colour (1550-V) and M_{g2} index essentially refer to the central parts of the galaxies (see Burstein et al. 1988), the integrated magnitudes and

colours, such as V, (B–V), (V–K) etc., refer to the whole galaxy. This is particularly true with the data we are using for galaxies in the Virgo and Coma cluster. The presence of spatial gradients of colours and metallicity that are known to exist in elliptical galaxies (Carollo et al. 1993, Carollo & Danziger 1994, Davies et al. 1993, Shombert et al. 1993) indicates that the one-zone models (either closed or with infall) ought to be abandoned in favor of models in which the spatial distribution of mass density and star formation rate is taken into account. It seems reasonable to argue that higher metallicities can be present in the central regions thus facilitating the formation of the right type of stellar source of the UV radiation (H-HB and AGB-manqué stars) whereas lower metallicities across the remaining parts of the galaxies would make it easier to fit the others integrated colours such as (V–K). Preliminary models of elliptical galaxies with spatial distribution of total mass and gas density, star formation rates, metallicities and colours are in progress (Tantalo 1994).

An alternative scenario has been proposed by Elbaz et al. (1995) aimed at explaining the amount of iron present in the intra-cluster medium. The goal is achieved by means of models for the evolution of elliptical galaxies with bimodal star formation. In brief, most of the heavy elements are supposed to be produced by SNII during a first violent phase during which only high-mass stars are formed. This is followed by a phase of quiescence caused by galactic winds. Finally, star formation is supposed to start again with normal IMF when sufficient gas has been made available by previously born stars. However, using the Elbaz et al. (1994) models Gibson (1995) has tried to reproduce the present-day photometric and chemical properties of elliptical galaxies with the conclusion that these models while successfully reproducing the observational data for the intra-cluster medium, fail to reproduce the chemo-spectro-photometric properties of the present day elliptical galaxies.

Acknowledgements

This work has been financially supported by the Italian Ministry of University, Scientific Research and Technology (MURST), the National Council of Research (CNR-GNA), and the Italian Space Agency (ASI).

References

- Alongi M., Bertelli G., Bressan A., Chiosi C., Fagotto F., Greggio L., Nasi E., 1993, *A&AS*, 97, 851
- Alfensleben U-F., Gerhard O.E. 1994, *A&A* 285, 751
- Angeletti L., Giannone P., 1990, *A&A*, 234, 53
- Arimoto N., Yoshii, Y. 1987, *A&A*, 173, 23
- Barbuy B. 1994, *ApJ* 430, 218
- Bender R., Burstein D., Faber S.M., 1992, *ApJ*, 399, 462
- Bender R., Burstein D., Faber S.M., 1993, *ApJ*, 411, 153
- Bertin G., Saglia R. P., Stiavelli M., 1992, *ApJ*, 384, 423
- Bertola F., Bressan A., Burstein D., Buson L., Chiosi C., di Serego Alighieri S., 1995, *ApJ* 438, 680
- Bessell M.S., Brett J.M., Scholz M., Wood P.R., 1989, *A&AS*, 77, 1
- Bessell M.S., Brett J.M., Scholz M., Wood P.R., 1991, *A&AS*, 89, 335
- Bower R. G., Lucey J. R., Ellis R.S., 1992a, *MNRAS*, 254, 589
- Bower R. G., Lucey J. R., Ellis R.S., 1992b, *MNRAS*, 254, 601
- Branch D., Tammann G.A., 1992, *ARA&A*, 30, 359
- Bressan A., Chiosi C., Fagotto F., 1994, *ApJS*, 94, 63
- Bressan A., Chiosi C., Tantalo R., 1995, *A&A* submitted
- Bressan A., Bertelli G., Fagotto F., Chiosi C., 1993, *A&AS*, 100, 647
- Brocato E., Matteucci F., Mazzitelli I., Tornambé A., 1990, *ApJ* 349, 458
- Bruzual G., 1992, in *The Stellar Populations of Galaxies*, B. Barbuy and A. Renzini (eds.), Kluwer Academic Publishers, Dordrecht, p. 311
- Bruzual G., Charlot S., 1993, *ApJ* 405, 538
- Burstein D., Bertola F., Buson L.M., Faber S.M., Lauer T.R., 1988, *ApJ* 328, 440
- Buzzoni A., Gariboldi G., Mantegazza L., 1992, *AJ* 103, 1814
- Carollo C.M., Danziger I.J., 1994, *MNRAS* 270, 523
- Carollo C.M., Danziger I.J., Buson L., 1993, *MNRAS*, 265, 553
- Charlot S., Bruzual G., 1991, *ApJ* 367, 126
- Chiosi C., 1981, *A&A* 83, 206
- Chiosi C., 1986, in *Nucleosynthesis and Stellar Evolution*, 16th Saas-Fee Course, B. Hauck, A. Maeder, and G. Meynet (eds.), Geneva, Geneva Obs., 199
- Chiosi C., Bressan A., 1995, *A&A* to be submitted
- Chiosi C., Bertelli G., Bressan A., 1992, *ARA&A* 30, 305
- Chiosi C., Maeder A., 1986, *ARA&A* 24, 329
- Cox D.P., 1972, *ApJ* 178, 159
- Davies R.L., Sadler E.M., Peletier R.F., 1993, *MNRAS* 262, 650
- Elbaz D., Arnaud M., Vangioni-Flam E., 1995, *A&A*, submitted
- Faber S.M., Burstein D., Dressler A., 1977, *AJ*, 82, 941
- Fagotto F., Bressan A., Bertelli G., Chiosi C., 1994a, *A&AS* 100, 647
- Fagotto F., Bressan A., Bertelli G., Chiosi C., 1994b, *A&AS* 104, 647
- Fagotto F., Bressan A., Bertelli G., Chiosi C., 1994b, *A&AS* 105, 39
- Ferguson H.C., Davidsen A.F., 1993, *ApJ* 408, 92
- Ferguson H.C., Davidsen A.F., Kriss G.A., Blair W.P., et al., 1991, *ApJ* 382, L69
- Fluks M.A., Plez B., Thé P.S., de Winter D., Westerlund B.E., Steenman H.C., 1994, *A&AS*, 105, 311
- Frogel J.A., Persson S.E., Aaronson M., Matthews K., 1978, *ApJ*, 220, 75
- Gibson B.K., 1995, *MNRAS*, submitted
- Gibson B.K., 1994, *MNRAS* 271, L35
- Greggio L., Renzini A., 1990, *ApJ* 364, 35
- Horch E., Demarque P., Pinsonneault M., 1992, *ApJ* 388, L53
- Kudritzki K.P., Pauldrach A., Puls J., 1987, *A&A* 173, 293
- Larson R.B., 1974, *MNRAS* 166, 585
- Larson R.B., 1991, in *Frontiers of Stellar Evolution*, D. L. Lambert (ed.), ASP Conference Series, Vol. 20, p. 571
- Lee Y-W., 1994, *ApJ* 423, 248

- Lynden-Bell D., 1975, *Vistas in Astronomy*, 19, 299
- Matteucci F. 1991, in *Frontiers of Stellar Evolution*, D. L. Lambert (ed.), ASP Conf. Ser. vol. 20, p. 539
- Matteucci F., 1994, *A&A* 228, 57
- Matteucci F., Tornambé A., 1987, *A&A* 185, 51
- Matthews W.G., Baker J.C., 1971, *ApJ* 170, 241
- Padovani P., Matteucci F., 1993, *ApJ* 416, 26
- Pagel B.E.J., 1989, in *Evolutionary Phenomena in Galaxies*, J. Beckman and B. E. J. Pagel (eds.), Cambridge, Cambridge University Press, p. 201
- Pagel B.E.J., Simonson E.A., Terlevich R.J., Edmunds M.G., 1992, *MNRAS* 255, 325
- Phillips S., 1993, *MNRAS* 263, 86
- Rana N. C., 1991, *ARA&A* 29, 129
- Renzini A., Buzzoni A., 1986, in *Spectral Evolution of Galaxies*, C. Chiosi and A. Renzini (eds.), Dordrecht, Reidel, p. 195
- Renzini A., Ciotti L., 1993, *ApJ* 416, L49
- Rigden S.T., Joyce R.R., White N.M., Wing R.F., 1980, *ApJ* 235, 126
- Saglia R. P., Bertin G., Stiavelli M., 1992, *ApJ* 384, 433
- Saito M., 1979a, *PASJ* 31, 181
- Saito M., 1979b, *PASJ* 31, 193
- Schmidt M., 1959, *ApJ* 129, 243
- Schombert J.M., Halan P.C., Barsony M., Rakos K.D., 1993, *AJ* 106, 923
- schweizer F., Seitzer P. 1992, *AJ* 104, 1039
- Silva L., 1995, Master thesis, University of Padua, Italy
- Tantalo R., 1994, Master thesis, University of Padua, Italy
- Terlevich R., Boyle B.J., 1993, *MNRAS*, in press
- Theis Ch., Burkert A., Hensler G., 1992, *A&A* 265, 465
- Tinsley B.M., 1980a, *ApJ* 241, 41
- Tinsley B.M., 1980b, *Fundamentals of Cosmic Physics* 5, 287
- Trimble V., 1991, *AAR* 3, 1
- Vader J.P., 1986, *ApJ* 306, 390
- VanderBerg D., 1985, *ApJS* 58, 711
- Worthey G., Faber S.M., Gonzales J.J., Burstein D., 1994, *ApJS* 94, 687

This article was processed by the author using Springer-Verlag
 \LaTeX A&A style file *L-AA* version 3.

Table 2: Integrated Colors of Single Stellar Populations

Age	M_V	M_{bol}	BC	(U-B)	(B-V)	(V-R)	(R-I)	(V-J)	(V-K)	(V-L)	(V-M)	(V-N)	(1550-V)
$Z = 0.0004$													
19.9526	5.042	4.658	-0.384	0.013	0.690	0.565	0.454	1.528	2.130	2.218	2.197	2.276	1.116
17.7828	4.927	4.578	-0.349	0.023	0.655	0.547	0.445	1.493	2.089	2.175	2.153	2.232	1.519
15.8489	4.813	4.501	-0.312	0.049	0.635	0.534	0.437	1.465	2.053	2.138	2.115	2.194	2.409
14.1254	4.620	4.324	-0.296	0.053	0.660	0.539	0.437	1.470	2.053	2.136	2.110	2.189	4.106
12.5893	4.542	4.244	-0.298	0.026	0.687	0.551	0.440	1.484	2.066	2.148	2.120	2.199	4.959
11.2202	4.469	4.170	-0.299	0.021	0.688	0.551	0.441	1.485	2.068	2.149	2.120	2.199	4.921
10.0000	4.379	4.075	-0.304	0.021	0.689	0.553	0.442	1.492	2.078	2.160	2.127	2.209	4.825
8.9125	4.238	3.935	-0.302	0.022	0.686	0.551	0.441	1.488	2.075	2.156	2.121	2.204	4.749
7.9433	4.160	3.859	-0.301	0.016	0.675	0.545	0.438	1.479	2.066	2.147	2.110	2.194	4.560
7.0795	4.089	3.788	-0.300	0.012	0.664	0.540	0.436	1.471	2.060	2.141	2.102	2.188	4.363
6.3096	3.933	3.627	-0.306	0.020	0.666	0.543	0.439	1.482	2.078	2.160	2.116	2.206	4.251
5.6234	3.853	3.551	-0.302	0.017	0.650	0.534	0.435	1.466	2.060	2.141	2.096	2.187	4.025
5.0119	3.782	3.484	-0.298	0.019	0.633	0.525	0.430	1.449	2.042	2.122	2.076	2.167	3.742
4.4668	3.640	3.338	-0.301	0.032	0.630	0.524	0.431	1.454	2.052	2.132	2.084	2.177	3.535
3.9811	3.564	3.268	-0.296	0.036	0.610	0.514	0.426	1.434	2.030	2.111	2.061	2.155	3.230
3.5481	3.463	3.162	-0.301	0.046	0.601	0.511	0.426	1.436	2.037	2.119	2.066	2.163	2.964
3.1623	3.347	3.049	-0.297	0.051	0.590	0.504	0.423	1.421	2.020	2.100	2.048	2.145	2.715
2.8184	3.275	2.981	-0.294	0.053	0.569	0.493	0.417	1.401	1.997	2.078	2.025	2.122	2.392
2.5119	3.127	2.826	-0.301	0.061	0.571	0.496	0.420	1.413	2.014	2.095	2.040	2.139	2.200
2.2387	3.053	2.753	-0.300	0.060	0.552	0.485	0.415	1.393	1.992	2.072	2.017	2.116	1.932
1.9953	2.884	2.574	-0.310	0.067	0.561	0.493	0.421	1.413	2.018	2.099	2.042	2.142	1.817
1.7783	2.820	2.512	-0.308	0.061	0.535	0.479	0.413	1.385	1.986	2.066	2.009	2.109	1.553
1.5849	2.763	2.451	-0.312	0.055	0.512	0.468	0.407	1.365	1.964	2.045	1.986	2.088	1.272
1.4125	2.657	2.332	-0.325	0.048	0.505	0.467	0.409	1.369	1.974	2.055	1.993	2.098	1.074
1.1220	2.414	2.063	-0.351	-0.013	0.440	0.433	0.397	1.338	2.024	2.112	2.015	2.151	0.781
1.0000	2.439	2.072	-0.367	-0.035	0.398	0.411	0.384	1.299	1.993	2.083	1.975	2.125	0.503
0.7943	2.248	1.842	-0.406	-0.051	0.369	0.403	0.385	1.304	2.019	2.113	1.992	2.156	0.234
0.6310	2.085	1.655	-0.430	-0.053	0.321	0.373	0.370	1.251	1.955	2.048	1.927	2.091	-0.065
0.5012	1.981	1.497	-0.485	-0.065	0.281	0.355	0.366	1.232	1.938	2.033	1.910	2.077	-0.393
0.3981	1.700	1.166	-0.534	-0.063	0.298	0.385	0.394	1.320	2.048	2.145	2.019	2.190	-0.483
0.3162	1.596	0.991	-0.605	-0.108	0.273	0.376	0.391	1.306	2.032	2.129	2.002	2.174	-0.791
0.2512	1.312	0.658	-0.654	-0.119	0.293	0.402	0.412	1.373	2.108	2.207	2.078	2.252	-0.889
0.1995	1.237	0.496	-0.741	-0.176	0.265	0.388	0.403	1.342	2.066	2.165	2.038	2.210	-1.188
0.1585	1.049	0.232	-0.817	-0.199	0.300	0.430	0.435	1.444	2.183	2.284	2.155	2.330	-1.314
0.1259	0.936	0.073	-0.863	-0.252	0.239	0.369	0.382	1.270	1.946	2.041	1.928	2.085	-1.544
0.1000	1.135	0.135	-1.000	-0.372	0.016	0.100	0.111	0.379	0.670	0.707	0.695	0.730	-2.051
0.0794	0.991	-0.128	-1.120	-0.416	-0.004	0.084	0.094	0.323	0.593	0.626	0.617	0.647	-2.233
0.0631	0.862	-0.383	-1.245	-0.460	-0.022	0.072	0.080	0.283	0.544	0.575	0.565	0.595	-2.408
0.0501	0.688	-0.658	-1.345	-0.494	-0.037	0.061	0.069	0.246	0.496	0.526	0.515	0.545	-2.539
0.0398	0.620	-0.910	-1.530	-0.553	-0.051	0.054	0.062	0.232	0.490	0.521	0.507	0.539	-2.773
0.0316	0.403	-1.202	-1.606	-0.578	-0.049	0.062	0.072	0.267	0.549	0.583	0.566	0.603	-2.856
0.0251	0.395	-1.459	-1.855	-0.658	-0.083	0.035	0.041	0.178	0.438	0.467	0.448	0.483	-3.154
0.0200	0.193	-1.749	-1.942	-0.689	-0.086	0.038	0.045	0.191	0.464	0.495	0.475	0.512	-3.247
0.0158	0.113	-2.026	-2.139	-0.747	-0.122	0.002	0.001	0.054	0.268	0.290	0.267	0.299	-3.462
0.0126	-0.054	-2.383	-2.329	-0.808	-0.179	-0.067	-0.090	-0.258	-0.246	-0.261	-0.284	-0.282	-3.658
0.0100	-0.142	-2.722	-2.580	-0.909	-0.219	-0.101	-0.145	-0.416	-0.471	-0.509	-0.541	-0.557	-3.901
0.0079	-0.266	-3.041	-2.775	-0.956	-0.238	-0.117	-0.169	-0.498	-0.613	-0.669	-0.704	-0.734	-4.049
0.0063	-0.600	-3.384	-2.785	-0.945	-0.231	-0.109	-0.157	-0.466	-0.573	-0.623	-0.653	-0.682	-4.016
0.0050	-1.075	-3.782	-2.707	-0.899	-0.127	0.019	0.014	0.097	0.302	0.326	0.331	0.335	-3.865
0.0040	-1.780	-4.162	-2.382	-0.670	0.031	0.133	0.138	0.441	0.671	0.707	0.720	0.735	-3.415
$Z = 0.004$													
19.9526	5.361	4.826	-0.535	0.191	0.742	0.617	0.539	1.792	2.572	2.693	2.580	2.758	1.023
17.7828	5.162	4.667	-0.495	0.302	0.772	0.625	0.543	1.808	2.591	2.707	2.581	2.767	3.090
15.8489	5.086	4.587	-0.499	0.305	0.871	0.656	0.547	1.840	2.617	2.730	2.602	2.791	3.764
14.1254	5.012	4.511	-0.501	0.316	0.884	0.659	0.549	1.847	2.631	2.743	2.608	2.805	4.138
12.5893	4.921	4.422	-0.499	0.312	0.880	0.657	0.551	1.850	2.637	2.748	2.612	2.805	5.286
11.2202	4.787	4.286	-0.501	0.307	0.876	0.654	0.552	1.855	2.644	2.753	2.615	2.804	6.047
10.0000	4.704	4.206	-0.497	0.287	0.862	0.646	0.550	1.848	2.637	2.746	2.609	2.792	6.173
8.9125	4.630	4.135	-0.496	0.270	0.848	0.639	0.547	1.843	2.634	2.743	2.609	2.785	6.252
7.9433	4.483	3.973	-0.510	0.272	0.850	0.641	0.552	1.865	2.669	2.778	2.641	2.818	6.255
7.0795	4.404	3.898	-0.506	0.250	0.832	0.631	0.548	1.857	2.662	2.771	2.639	2.812	6.243
6.3096	4.326	3.827	-0.499	0.231	0.815	0.622	0.542	1.843	2.647	2.756	2.627	2.796	6.117
5.6234	4.216	3.716	-0.499	0.224	0.807	0.618	0.542	1.842	2.648	2.757	2.629	2.794	5.996
5.0119	4.135	3.644	-0.491	0.208	0.792	0.610	0.536	1.826	2.631	2.740	2.613	2.777	5.849
4.4668	4.058	3.575	-0.483	0.193	0.775	0.601	0.531	1.810	2.612	2.721	2.596	2.756	5.671
3.9811	3.923	3.434	-0.490	0.197	0.775	0.600	0.533	1.820	2.628	2.737	2.611	2.772	5.568
3.5481	3.842	3.363	-0.479	0.183	0.758	0.591	0.527	1.800	2.605	2.713	2.589	2.746	5.418
3.1623	3.682	3.175	-0.507	0.193	0.762	0.595	0.540	1.843	2.668	2.778	2.653	2.809	5.260
2.8184	3.545	3.048	-0.496	0.199	0.760	0.592	0.535	1.828	2.644	2.753	2.630	2.784	5.136
2.5119	3.463	2.989	-0.474	0.167	0.718	0.570	0.521	1.783	2.594	2.704	2.584	2.735	4.786
2.2387	3.413	2.946	-0.466	0.148	0.695	0.557	0.514	1.763	2.575	2.685	2.567	2.717	4.624
1.9953	3.287	2.812	-0.476	0.150	0.671	0.547	0.516	1.771	2.595	2.708	2.591	2.738	4.246
1.7783	3.185	2.731	-0.453	0.154	0.638	0.526	0.503	1.726	2.542	2.653	2.538	2.682	3.850
1.5849	3.059	2.591	-0.468	0.161	0.614	0.515	0.508	1.742	2.576	2.689	2.575	2.717	3.503
1.4454	2.922	2.417	-0.505	0.174	0.605	0.514	0.525	1.796	2.660	2.778	2.666	2.805	3.263
1.1220	2.636	2.236	-0.400	0.157	0.528	0.453	0.465	1.596	2.403	2.511	2.399	2.527	2.485
1.0000	2.616	2.189	-0.427	0.130	0.459	0.416	0.463	1.605	2.456	2.572	2.468	2.593	1.988
0.7943	2.456	2.017	-0.439	0.102	0.383	0.371	0.443	1.562	2.429	2.555	2.471	2.588	1.178

Table 2: Integrated Colors of SSPs *continued*

Age	M_V	M_{bol}	BC	(U-B)	(B-V)	(V-R)	(R-I)	(V-J)	(V-K)	(V-L)	(V-M)	(V-N)	(1550-V)
0.6310	2.326	1.870	-0.456	0.054	0.313	0.326	0.414	1.497	2.372	2.508	2.444	2.560	0.515
0.5012	2.127	1.614	-0.513	0.012	0.304	0.337	0.438	1.529	2.413	2.537	2.438	2.558	0.118
0.3981	1.960	1.415	-0.545	-0.045	0.267	0.324	0.438	1.469	2.341	2.456	2.324	2.448	-0.255
0.3162	1.709	1.066	-0.643	-0.086	0.279	0.352	0.492	1.603	2.519	2.638	2.495	2.622	-0.464
0.2512	1.546	0.854	-0.693	-0.147	0.228	0.320	0.476	1.547	2.467	2.587	2.439	2.567	-0.775
0.1995	1.437	0.671	-0.766	-0.188	0.183	0.293	0.471	1.521	2.454	2.576	2.420	2.557	-1.061
0.1585	1.196	0.360	-0.836	-0.193	0.200	0.330	0.517	1.613	2.559	2.682	2.512	2.661	-1.172
0.1259	1.098	0.195	-0.903	-0.256	0.167	0.313	0.484	1.504	2.427	2.547	2.363	2.534	-1.463
0.1000	1.003	0.185	-0.818	-0.305	0.113	0.200	0.223	0.757	1.252	1.320	1.196	1.343	-1.699
0.0794	0.919	-0.049	-0.968	-0.371	0.081	0.180	0.208	0.713	1.206	1.274	1.146	1.296	-1.969
0.0631	0.741	-0.328	-1.068	-0.397	0.088	0.195	0.227	0.773	1.294	1.366	1.228	1.390	-2.113
0.0501	0.530	-0.623	-1.153	-0.411	0.116	0.230	0.263	0.886	1.447	1.524	1.374	1.551	-2.215
0.0398	0.451	-0.868	-1.319	-0.474	0.109	0.234	0.270	0.912	1.492	1.572	1.412	1.599	-2.449
0.0316	0.191	-1.172	-1.362	-0.472	0.126	0.260	0.301	1.004	1.619	1.703	1.530	1.733	-2.481
0.0251	0.139	-1.430	-1.569	-0.582	0.036	0.188	0.238	0.818	1.413	1.496	1.316	1.523	-2.773
0.0200	-0.036	-1.720	-1.684	-0.642	0.017	0.181	0.233	0.811	1.418	1.502	1.315	1.530	-2.911
0.0158	-0.030	-1.996	-1.966	-0.754	-0.069	0.092	0.137	0.525	1.058	1.134	0.955	1.155	-3.265
0.0126	-0.461	-2.354	-1.893	-0.701	-0.022	0.142	0.193	0.682	1.242	1.324	1.142	1.350	-3.152
0.0100	-0.891	-2.672	-1.781	-0.629	0.043	0.197	0.241	0.811	1.361	1.443	1.275	1.471	-2.983
0.0079	-1.140	-3.015	-1.875	-0.637	-0.052	0.061	0.077	0.262	0.525	0.569	0.493	0.582	-3.098
0.0063	-1.449	-3.349	-1.901	-0.662	-0.125	-0.033	-0.046	-0.163	-0.186	-0.196	-0.202	-0.210	-3.102
0.0050	-1.095	-3.737	-2.643	-0.931	-0.202	-0.083	-0.120	-0.347	-0.394	-0.427	-0.448	-0.469	-3.863
0.0040	-1.164	-4.136	-2.973	-0.914	-0.191	-0.069	-0.097	-0.282	-0.300	-0.322	-0.337	-0.352	-3.935
<hr/>													
$Z = 0.008$													
16.5959	5.382	4.755	-0.627	0.439	0.928	0.689	0.593	2.045	2.897	3.025	2.907	3.078	3.612
15.8489	5.354	4.730	-0.624	0.440	0.932	0.689	0.590	2.041	2.897	3.025	2.901	3.083	3.715
14.1254	5.217	4.577	-0.640	0.454	0.941	0.693	0.599	2.067	2.931	3.056	2.926	3.104	4.036
12.5893	5.128	4.497	-0.631	0.436	0.930	0.688	0.596	2.058	2.919	3.044	2.919	3.089	4.707
11.2202	5.042	4.424	-0.618	0.414	0.919	0.680	0.589	2.042	2.902	3.028	2.908	3.079	5.942
10.0000	4.918	4.295	-0.623	0.402	0.915	0.677	0.587	2.048	2.917	3.046	2.927	3.104	6.117
8.9125	4.830	4.215	-0.615	0.377	0.899	0.668	0.581	2.035	2.904	3.036	2.925	3.099	6.282
7.9433	4.694	4.072	-0.622	0.368	0.895	0.666	0.581	2.044	2.920	3.056	2.950	3.126	6.361
7.0795	4.604	3.992	-0.612	0.344	0.878	0.657	0.575	2.028	2.902	3.040	2.941	3.112	6.485
6.3096	4.520	3.920	-0.601	0.319	0.862	0.648	0.567	2.009	2.882	3.021	2.922	3.095	6.563
5.6234	4.444	3.856	-0.588	0.297	0.846	0.639	0.560	1.988	2.859	2.997	2.900	3.072	6.571
5.0119	4.379	3.805	-0.574	0.273	0.827	0.628	0.552	1.964	2.829	2.967	2.872	3.040	6.494
4.4668	4.298	3.734	-0.565	0.256	0.814	0.621	0.546	1.949	2.813	2.950	2.855	3.025	6.399
3.9811	4.223	3.668	-0.555	0.243	0.802	0.614	0.541	1.932	2.792	2.928	2.834	3.001	6.301
3.5481	3.905	3.264	-0.642	0.311	0.857	0.650	0.578	2.063	2.965	3.105	3.000	3.178	6.179
3.1623	3.954	3.390	-0.564	0.251	0.804	0.615	0.543	1.945	2.813	2.948	2.850	3.021	6.094
2.8184	3.772	3.181	-0.591	0.250	0.804	0.618	0.551	1.983	2.870	3.009	2.910	3.084	5.993
2.5119	3.679	3.104	-0.575	0.244	0.793	0.611	0.544	1.959	2.836	2.974	2.878	3.047	5.870
2.2387	3.568	3.009	-0.559	0.207	0.755	0.592	0.534	1.927	2.803	2.940	2.847	3.013	5.568
1.9953	3.498	2.953	-0.545	0.182	0.728	0.577	0.526	1.901	2.774	2.913	2.825	2.985	5.377
1.7783	3.268	2.697	-0.571	0.202	0.736	0.583	0.537	1.942	2.828	2.968	2.880	3.039	5.143
1.5849	3.150	2.601	-0.549	0.182	0.698	0.560	0.525	1.903	2.785	2.925	2.844	2.995	4.777
1.4125	3.027	2.454	-0.573	0.169	0.663	0.542	0.530	1.931	2.838	2.986	2.916	3.061	4.393
1.1220	2.767	2.310	-0.457	0.170	0.575	0.473	0.468	1.732	2.592	2.738	2.685	2.817	3.547
1.0000	2.744	2.306	-0.439	0.149	0.505	0.427	0.450	1.675	2.545	2.695	2.652	2.775	3.026
0.7943	2.574	2.153	-0.421	0.138	0.412	0.372	0.425	1.594	2.471	2.622	2.579	2.700	2.109
0.6310	2.396	1.931	-0.465	0.116	0.349	0.341	0.431	1.612	2.523	2.678	2.632	2.753	1.292
0.5012	2.231	1.745	-0.486	0.077	0.302	0.317	0.423	1.576	2.489	2.639	2.589	2.705	0.656
0.3981	2.051	1.450	-0.602	0.024	0.260	0.308	0.463	1.701	2.672	2.828	2.773	2.889	0.134
0.3162	1.851	1.228	-0.623	-0.034	0.240	0.297	0.447	1.650	2.607	2.758	2.703	2.812	-0.236
0.2512	1.700	1.025	-0.675	-0.109	0.195	0.268	0.432	1.605	2.566	2.717	2.662	2.765	-0.615
0.1995	1.591	0.840	-0.751	-0.177	0.162	0.247	0.426	1.598	2.571	2.721	2.667	2.765	-0.934
0.1585	1.345	0.489	-0.856	-0.213	0.178	0.277	0.487	1.748	2.753	2.898	2.826	2.921	-1.092
0.1259	1.219	0.297	-0.922	-0.265	0.127	0.242	0.475	1.677	2.680	2.818	2.724	2.819	-1.374
0.1000	1.050	0.309	-0.741	-0.293	0.099	0.181	0.197	0.716	1.226	1.295	1.151	1.319	-1.565
0.0794	0.953	0.075	-0.879	-0.353	0.057	0.154	0.178	0.657	1.165	1.234	1.083	1.258	-1.832
0.0631	0.784	-0.210	-0.995	-0.395	0.051	0.162	0.192	0.709	1.259	1.334	1.167	1.359	-2.010
0.0501	0.588	-0.510	-1.099	-0.426	0.058	0.184	0.220	0.807	1.410	1.491	1.307	1.520	-2.147
0.0398	0.494	-0.766	-1.259	-0.488	0.033	0.171	0.214	0.793	1.414	1.498	1.304	1.528	-2.382
0.0316	0.241	-1.077	-1.318	-0.497	0.060	0.213	0.261	0.946	1.625	1.717	1.508	1.751	-2.426
0.0251	0.139	-1.362	-1.501	-0.579	0.010	0.170	0.222	0.829	1.491	1.583	1.371	1.615	-2.686
0.0200	-0.081	-1.652	-1.571	-0.604	0.009	0.176	0.229	0.855	1.528	1.622	1.405	1.655	-2.762
0.0158	-0.161	-1.947	-1.787	-0.696	-0.051	0.113	0.162	0.651	1.274	1.364	1.151	1.393	-3.044
0.0126	-0.454	-2.292	-1.839	-0.706	-0.050	0.115	0.164	0.652	1.264	1.353	1.142	1.383	-3.094
0.0100	-0.610	-2.558	-1.947	-0.736	-0.016	0.162	0.209	0.796	1.429	1.523	1.309	1.553	-3.200
0.0079	-1.188	-2.967	-1.779	-0.626	0.072	0.197	0.207	0.737	1.185	1.257	1.119	1.281	-2.980
0.0063	-1.721	-3.287	-1.566	-0.486	0.088	0.153	0.148	0.482	0.730	0.774	0.750	0.796	-2.698
0.0050	-1.278	-3.703	-2.425	-0.893	-0.179	-0.056	-0.087	-0.218	-0.157	-0.161	-0.221	-0.189	-3.641
<hr/>													
$Z = 0.02$													
19.9526	5.829	4.984	-0.845	0.598	1.004	0.730	0.662	2.356	3.307	3.543	3.542	3.713	3.586
17.7828	5.718	4.848	-0.870	0.668	1.045	0.743	0.667	2.391	3.349	3.589	3.591	3.766	3.583
15.8489	5.630	4.781	-0.850	0.653	1.038	0.739	0.660	2.365	3.315	3.552	3.552	3.726	3.716
14.1254	5.548	4.713	-0.835	0.633	1.030	0.734	0.654	2.347	3.295	3.532	3.531	3.706	4.141
12.5893	5.467	4.640	-0.827	0.608	1.017	0.726	0.650	2.340	3.290	3.531	3.534	3.708	5.248
11.2202	5.325	4.484	-0.841	0.598	1.014	0.725	0.655	2.359	3.319	3.564	3.567	3.740	5.869

Table 2: Integrated Colors of SSPs *continued*

Age	M_V	M_{bol}	BC	(U-B)	(B-V)	(V-R)	(R-I)	(V-J)	(V-K)	(V-L)	(V-M)	(V-N)	(1550-V)
10.0000	5.237	4.403	-0.834	0.565	0.996	0.715	0.649	2.348	3.310	3.561	3.573	3.744	6.049
8.9125	5.156	4.329	-0.827	0.533	0.979	0.705	0.644	2.337	3.302	3.555	3.569	3.739	6.221
7.9433	5.055	4.229	-0.826	0.511	0.967	0.699	0.643	2.334	3.302	3.557	3.574	3.741	6.346
7.0795	4.967	4.156	-0.811	0.484	0.952	0.691	0.637	2.314	3.279	3.534	3.550	3.718	6.490
6.3096	4.885	4.087	-0.798	0.458	0.937	0.683	0.631	2.295	3.257	3.513	3.530	3.696	6.621
5.6234	4.709	3.877	-0.832	0.468	0.946	0.689	0.643	2.339	3.316	3.576	3.594	3.761	6.609
5.0119	4.619	3.806	-0.812	0.442	0.930	0.679	0.635	2.312	3.285	3.543	3.561	3.727	6.681
4.4668	4.461	3.613	-0.848	0.438	0.930	0.683	0.649	2.357	3.345	3.608	3.629	3.793	6.608
3.9811	4.347	3.527	-0.820	0.423	0.918	0.674	0.637	2.320	3.299	3.558	3.577	3.742	6.694
3.5481	4.241	3.457	-0.784	0.386	0.893	0.659	0.622	2.270	3.240	3.496	3.514	3.677	6.772
3.1623	4.160	3.402	-0.759	0.346	0.866	0.645	0.612	2.232	3.196	3.453	3.470	3.632	6.818
2.8184	4.074	3.309	-0.765	0.316	0.845	0.634	0.610	2.237	3.212	3.479	3.505	3.668	6.726
2.5119	3.958	3.218	-0.740	0.296	0.829	0.626	0.601	2.200	3.166	3.432	3.456	3.620	6.964
2.2387	3.835	3.105	-0.730	0.272	0.807	0.614	0.592	2.183	3.150	3.423	3.455	3.619	6.841
1.9953	3.720	3.008	-0.712	0.248	0.785	0.604	0.583	2.155	3.118	3.392	3.427	3.590	6.661
1.7783	3.566	2.853	-0.713	0.240	0.774	0.597	0.578	2.154	3.122	3.403	3.443	3.608	6.420
1.5849	3.444	2.750	-0.694	0.220	0.747	0.580	0.563	2.123	3.090	3.380	3.431	3.594	6.171
1.4125	3.335	2.668	-0.667	0.198	0.716	0.560	0.545	2.082	3.044	3.341	3.403	3.561	5.848
1.0000	2.928	2.339	-0.589	0.178	0.617	0.487	0.494	1.954	2.909	3.225	3.317	3.460	4.676
0.7943	2.769	2.226	-0.544	0.165	0.510	0.418	0.459	1.857	2.819	3.149	3.254	3.393	3.720
0.6310	2.553	2.021	-0.532	0.163	0.420	0.364	0.436	1.804	2.783	3.124	3.239	3.377	2.797
0.5012	2.361	1.848	-0.512	0.139	0.330	0.308	0.404	1.718	2.702	3.051	3.174	3.311	1.858
0.3981	2.160	1.551	-0.609	0.100	0.276	0.286	0.425	1.821	2.853	3.222	3.357	3.495	1.022
0.3162	1.976	1.345	-0.631	0.041	0.223	0.257	0.408	1.775	2.809	3.181	3.317	3.456	0.359
0.2512	1.833	1.156	-0.677	-0.037	0.168	0.225	0.390	1.738	2.782	3.159	3.300	3.439	-0.184
0.1995	1.701	0.834	-0.867	-0.110	0.142	0.223	0.455	1.983	3.093	3.490	3.643	3.783	-0.575
0.1585	1.508	0.607	-0.902	-0.172	0.139	0.233	0.450	1.948	3.044	3.429	3.571	3.712	-0.859
0.1259	1.376	0.409	-0.966	-0.249	0.108	0.216	0.440	1.913	3.010	3.387	3.522	3.663	-1.182
0.1000	1.199	0.159	-1.039	-0.302	0.120	0.243	0.463	1.933	3.020	3.366	3.476	3.619	-1.410
0.0794	1.068	0.014	-1.055	-0.369	0.092	0.225	0.416	1.717	2.756	3.040	3.096	3.241	-1.680
0.0631	0.891	-0.048	-0.939	-0.413	0.099	0.222	0.259	0.937	1.586	1.674	1.476	1.703	-1.869
0.0501	0.704	-0.338	-1.043	-0.448	0.111	0.242	0.282	1.012	1.700	1.792	1.584	1.828	-2.023
0.0398	0.574	-0.625	-1.199	-0.510	0.073	0.222	0.280	1.011	1.737	1.836	1.614	1.874	-2.264
0.0316	0.483	-0.871	-1.354	-0.563	0.053	0.225	0.306	1.094	1.883	1.990	1.750	2.034	-2.466
0.0251	0.263	-1.220	-1.483	-0.608	0.071	0.262	0.352	1.234	2.064	2.177	1.927	2.223	-2.608
0.0200	0.174	-1.468	-1.642	-0.669	0.043	0.250	0.355	1.243	2.095	2.211	1.954	2.259	-2.813
0.0158	-0.133	-1.816	-1.683	-0.666	0.080	0.286	0.391	1.342	2.208	2.327	2.069	2.377	-2.837
0.0126	-0.493	-2.147	-1.654	-0.617	0.109	0.301	0.397	1.353	2.200	2.319	2.065	2.369	-2.780
0.0100	-0.582	-2.469	-1.887	-0.756	0.141	0.348	0.409	1.410	2.220	2.336	2.083	2.382	-3.074
0.0079	-1.343	-2.877	-1.534	-0.562	0.281	0.321	0.288	0.996	1.485	1.561	1.440	1.591	-2.672
0.0063	-1.352	-3.178	-1.826	-0.712	-0.060	0.069	0.081	0.338	0.682	0.740	0.599	0.753	-3.056
0.0050	-1.116	-3.558	-2.442	-0.914	-0.204	-0.092	-0.139	-0.403	-0.478	-0.519	-0.563	-0.578	-3.631
0.0040	-1.570	-3.920	-2.350	-0.894	-0.206	-0.099	-0.151	-0.457	-0.590	-0.647	-0.681	-0.717	-3.530
$Z = 0.05$													
19.9526	5.962	5.039	-0.923	0.479	0.745	0.642	0.659	2.434	3.450	3.782	3.871	4.035	2.876
17.7828	5.998	4.986	-1.012	0.958	1.119	0.778	0.701	2.591	3.590	3.897	3.960	4.133	4.701
15.8489	5.939	4.907	-1.032	0.966	1.128	0.792	0.715	2.614	3.617	3.914	3.963	4.140	5.761
14.1254	5.884	4.831	-1.054	0.932	1.119	0.791	0.723	2.639	3.652	3.950	3.998	4.175	5.552
12.5893	5.814	4.735	-1.080	0.892	1.105	0.786	0.729	2.668	3.695	4.005	4.063	4.238	4.984
11.2202	5.737	4.658	-1.079	0.862	1.094	0.779	0.728	2.667	3.699	4.010	4.071	4.244	5.654
10.0000	5.562	4.417	-1.145	0.866	1.101	0.786	0.749	2.745	3.799	4.121	4.191	4.362	5.706
8.9125	5.460	4.329	-1.131	0.829	1.086	0.776	0.742	2.727	3.781	4.106	4.177	4.348	5.892
7.9433	5.366	4.249	-1.117	0.791	1.070	0.767	0.735	2.710	3.764	4.091	4.165	4.335	6.086
6.3096	5.103	3.961	-1.142	0.751	1.056	0.759	0.741	2.739	3.805	4.140	4.221	4.389	6.291
5.6234	5.004	3.871	-1.133	0.709	1.037	0.748	0.735	2.727	3.795	4.134	4.219	4.385	6.310
4.4668	4.814	3.713	-1.101	0.643	1.006	0.729	0.721	2.687	3.753	4.092	4.179	4.344	6.458
3.9811	4.603	3.431	-1.172	0.662	1.023	0.742	0.747	2.771	3.855	4.202	4.293	4.458	6.368
3.1623	4.434	3.376	-1.058	0.522	0.944	0.693	0.700	2.628	3.695	4.040	4.132	4.295	6.601
2.8184	4.371	3.333	-1.038	0.502	0.933	0.686	0.693	2.603	3.666	4.011	4.104	4.266	6.656
2.5119	4.237	3.212	-1.025	0.472	0.917	0.678	0.687	2.586	3.648	3.993	4.085	4.247	6.956
2.2387	4.132	3.146	-0.986	0.429	0.890	0.662	0.671	2.534	3.589	3.930	4.022	4.182	7.007
1.9953	3.942	2.932	-1.011	0.427	0.892	0.666	0.680	2.565	3.628	3.971	4.063	4.225	6.977
1.5849	3.698	2.657	-1.040	0.359	0.841	0.637	0.673	2.597	3.682	4.060	4.182	4.340	6.860
1.4454	3.550	2.568	-0.982	0.358	0.835	0.629	0.646	2.525	3.593	3.968	4.091	4.248	7.003
1.0000	3.184	2.343	-0.841	0.256	0.725	0.555	0.576	2.331	3.380	3.763	3.900	4.049	6.591
0.7943	2.986	2.205	-0.781	0.193	0.631	0.501	0.544	2.235	3.282	3.671	3.813	3.961	5.510
0.6310	2.774	1.987	-0.787	0.193	0.538	0.448	0.535	2.226	3.295	3.698	3.850	3.997	4.364
0.5012	2.563	1.811	-0.752	0.192	0.458	0.402	0.513	2.157	3.228	3.634	3.789	3.935	3.372
0.3981	2.367	1.649	-0.718	0.164	0.354	0.339	0.484	2.071	3.149	3.563	3.722	3.868	2.375
0.3162	2.153	1.297	-0.855	0.129	0.302	0.324	0.532	2.237	3.359	3.789	3.958	4.104	1.485
0.2512	1.963	1.103	-0.860	0.061	0.228	0.282	0.513	2.184	3.312	3.745	3.916	4.062	0.673
0.1995	1.818	0.933	-0.885	-0.016	0.170	0.247	0.498	2.145	3.280	3.715	3.887	4.033	0.054
0.1585	1.675	0.588	-1.087	-0.088	0.141	0.247	0.581	2.395	3.573	4.023	4.204	4.350	-0.369
0.1259	1.497	0.370	-1.127	-0.161	0.121	0.247	0.580	2.383	3.560	4.006	4.182	4.330	-0.716
0.1000	1.365	0.185	-1.180	-0.243	0.083	0.223	0.574	2.364	3.547	3.993	4.168	4.317	-1.059
0.0794	1.206	-0.092	-1.299	-0.303	0.085	0.250	0.626	2.479	3.671	4.112	4.281	4.433	-1.314
0.0631	1.068	-0.201	-1.269	-0.377	0.048	0.219	0.557	2.264	3.436	3.861	4.014	4.171	-1.610
0.0501	0.918	-0.077	-0.995	-0.433	0.043	0.211	0.345	1.223	2.091	2.216	1.986	2.270	-1.836
0.0398	0.794	-0.346	-1.140	-0.496	0.006	0.187	0.362	1.248	2.154	2.278	2.046	2.308	-2.088
0.0316	0.619	-0.680	-1.300	-0.551	-0.006	0.193	0.416	1.402	2.373	2.507	2.272	2.545	-2.296
0.0251	0.513	-0.937	-1.450	-0.607	-0.043	0.157	0.423	1.431	2.438	2.582	2.368	2.620	-2.514

Table 2: Integrated Colors of SSPs *continued*

Age	M_V	M_{bol}	BC	(U-B)	(B-V)	(V-R)	(R-I)	(V-J)	(V-K)	(V-L)	(V-M)	(V-N)	(1550-V)
0.0200	0.323	-1.302	-1.625	-0.653	-0.044	0.188	0.550	1.747	2.824	2.982	2.795	3.024	-2.671
0.0158	0.192	-1.583	-1.774	-0.708	-0.094	0.147	0.560	1.722	2.805	2.968	2.844	2.975	-2.882
0.0126	0.028	-1.926	-1.954	-0.749	-0.103	0.194	0.735	2.081	3.208	3.389	3.310	3.391	-3.022
0.0100	-0.182	-2.225	-2.044	-0.800	-0.120	0.166	0.674	1.922	3.030	3.182	3.070	3.141	-3.178
0.0079	-0.595	-2.627	-2.032	-0.822	-0.001	0.292	0.633	1.933	3.008	3.157	2.894	3.201	-3.152
0.0063	-2.073	-3.160	-1.087	-0.325	0.314	0.314	0.278	0.964	1.393	1.470	1.342	1.500	-2.034
0.0050	-1.348	-3.530	-2.182	-0.919	-0.213	-0.106	-0.162	-0.484	-0.620	-0.682	-0.726	-0.763	-3.483
0.0040	-1.388	-3.679	-2.291	-0.900	-0.210	-0.104	-0.159	-0.478	-0.620	-0.682	-0.720	-0.760	-3.464
<hr/>													
$Z = 0.1$													
12.8825	6.253	4.469	-1.784	0.113	0.495	0.778	0.926	3.226	4.349	4.746	4.875	5.035	-1.238
12.5893	6.203	4.447	-1.755	0.087	0.470	0.761	0.912	3.185	4.305	4.701	4.829	4.990	-1.247
11.2202	5.948	4.326	-1.622	0.059	0.430	0.722	0.848	3.008	4.105	4.492	4.613	4.775	-1.243
10.0000	5.726	4.152	-1.575	0.040	0.428	0.717	0.830	2.941	4.022	4.400	4.509	4.675	-1.292
8.9125	5.516	4.088	-1.428	0.041	0.394	0.685	0.788	2.807	3.864	4.229	4.326	4.497	-1.040
7.9433	5.344	4.017	-1.327	0.097	0.401	0.686	0.791	2.765	3.800	4.144	4.214	4.397	-0.635
7.0795	5.164	3.853	-1.311	0.114	0.386	0.673	0.801	2.780	3.823	4.166	4.233	4.416	-0.378
6.3096	4.914	3.799	-1.114	0.288	0.409	0.665	0.759	2.667	3.682	4.009	4.062	4.248	3.033
5.6234	5.145	3.718	-1.427	0.501	0.609	0.827	0.918	3.077	4.113	4.431	4.457	4.661	6.378
5.0119	5.208	3.691	-1.517	0.416	0.566	0.816	0.967	3.179	4.240	4.559	4.585	4.788	6.311
4.4668	5.104	3.562	-1.542	0.382	0.561	0.820	0.984	3.201	4.274	4.587	4.613	4.804	6.339
3.9811	5.035	3.511	-1.524	0.328	0.535	0.801	0.973	3.178	4.255	4.564	4.588	4.775	6.434
3.5481	4.945	3.392	-1.552	0.292	0.521	0.792	0.979	3.208	4.299	4.614	4.649	4.830	6.460
3.1623	4.828	3.251	-1.577	0.275	0.513	0.784	0.982	3.236	4.336	4.659	4.706	4.885	6.621
2.8184	4.724	3.153	-1.571	0.238	0.498	0.769	0.974	3.226	4.333	4.668	4.727	4.903	6.663
2.5119	4.599	2.961	-1.638	0.222	0.493	0.766	1.000	3.301	4.425	4.777	4.853	5.025	6.619
2.2387	4.480	2.828	-1.651	0.201	0.483	0.755	1.000	3.314	4.446	4.809	4.899	5.068	6.740
1.5849	3.976	2.570	-1.406	0.157	0.462	0.708	0.901	3.027	4.117	4.446	4.500	4.677	6.204
1.2589	3.759	2.442	-1.317	0.122	0.439	0.673	0.857	2.913	3.997	4.332	4.394	4.568	6.473
1.0000	3.502	2.125	-1.378	0.115	0.418	0.645	0.870	2.984	4.095	4.457	4.547	4.717	6.352
0.7943	3.278	1.975	-1.303	0.092	0.362	0.580	0.822	2.886	4.002	4.377	4.482	4.651	5.874
0.6310	3.069	1.883	-1.186	0.097	0.311	0.523	0.773	2.726	3.838	4.217	4.326	4.489	4.873
0.5012	2.841	1.596	-1.245	0.123	0.277	0.494	0.801	2.794	3.927	4.319	4.439	4.600	3.757
0.3981	2.629	1.431	-1.198	0.118	0.214	0.427	0.773	2.717	3.857	4.257	4.385	4.544	2.680
0.3162	2.452	1.286	-1.166	0.095	0.160	0.368	0.749	2.652	3.799	4.206	4.339	4.498	1.808
0.2512	2.272	0.952	-1.321	0.067	0.126	0.352	0.828	2.833	4.006	4.424	4.565	4.725	1.052
0.1995	2.097	0.769	-1.328	0.007	0.075	0.302	0.819	2.801	3.983	4.402	4.544	4.703	0.278
0.1585	1.947	0.411	-1.536	-0.058	0.039	0.288	0.922	3.031	4.247	4.680	4.836	4.988	-0.319
0.1259	1.771	0.183	-1.588	-0.126	0.008	0.269	0.939	3.049	4.270	4.699	4.853	5.004	-0.804
0.1000	1.630	0.012	-1.618	-0.207	-0.029	0.231	0.926	3.019	4.253	4.684	4.843	4.987	-1.214
0.0794	1.515	-0.144	-1.659	-0.284	-0.055	0.206	0.917	2.995	4.244	4.675	4.842	4.974	-1.548
0.0631	1.406	-0.609	-2.015	-0.346	-0.079	0.214	1.142	3.443	4.718	5.163	5.341	5.474	-1.830
0.0501	1.238	-0.816	-2.054	-0.418	-0.112	0.148	1.098	3.414	4.696	5.154	5.343	5.479	-2.135
0.0398	1.115	-0.370	-1.485	-0.477	-0.138	0.026	0.432	2.114	3.323	3.713	3.874	4.002	-2.382
0.0316	0.968	-0.684	-1.652	-0.533	-0.153	0.010	0.457	2.246	3.480	3.967	4.179	4.317	-2.597
0.0251	0.831	-0.961	-1.793	-0.583	-0.165	0.002	0.488	2.320	3.562	4.055	4.269	4.407	-2.785
0.0200	0.662	-1.356	-2.019	-0.636	-0.178	0.008	0.636	2.635	3.899	4.396	4.611	4.750	-2.972
0.0158	0.483	-1.772	-2.255	-0.690	-0.190	0.020	0.813	2.968	4.248	4.747	4.964	5.103	-3.153
0.0126	0.279	-2.076	-2.355	-0.750	-0.206	0.002	0.771	2.888	4.167	4.666	4.882	5.022	-3.343

Table 5: Chemical Models at the Stage of Wind Ejection

ν	ζ	$M_L(0)$	$t_{q\omega}$	G(t)	S(t)	Z(t)	$\langle Z(t) \rangle$	Ψ	Ω_g	E_g	E_{SNI}	$E_{SNI I}$	E_{SW}
$k = 1 \quad t_{c\omega} = 15 \times 10^6 \text{ yr and } \tau = 0.10$													
12.0	0.50	3.000	0.26	0.232	0.696	0.0710	0.0360	8.25E+03	2.60E+10	2.65E+10	1.53E+08	1.64E+09	2.47E+10
7.2	0.50	1.000	0.31	0.312	0.648	0.0629	0.0307	2.22E+03	7.13E+09	7.40E+09	3.72E+07	3.35E+08	7.03E+09
5.2	0.50	0.500	0.35	0.381	0.589	0.0543	0.0265	9.82E+02	3.20E+09	3.23E+09	1.39E+07	1.19E+08	3.10E+09
3.0	0.50	0.100	0.34	0.560	0.408	0.0328	0.0166	1.67E+02	4.55E+08	4.67E+08	1.15E+06	1.11E+07	4.55E+08
2.5	0.50	0.050	0.29	0.640	0.310	0.0235	0.0122	7.97E+01	1.90E+08	1.93E+08	3.28E+05	3.84E+06	1.89E+08
1.0	0.50	0.010	0.43	0.768	0.218	0.0158	0.0080	7.67E+00	2.22E+07	2.25E+07	3.63E+04	2.95E+05	2.21E+07

Evolution of the Integrated Colours of the Model Galaxies

ν	ζ	$M_L(T_G)$	Age	M_{bol}	M_V	(U-B)	(B-V)	(V-R)	(V-K)	(1550-V)
12.00	0.50	3.000	17.0000	-24.616	-23.696	0.605	0.998	0.742	3.406	2.064
7.20	0.50	1.000	17.0000	-23.366	-22.501	0.596	1.000	0.735	3.329	2.713
5.20	0.50	0.500	17.0000	-22.517	-21.697	0.576	0.995	0.728	3.261	3.401
3.00	0.50	0.100	17.0000	-20.402	-19.673	0.475	0.948	0.704	3.093	3.365
2.50	0.50	0.050	17.0000	-19.363	-18.690	0.418	0.916	0.690	2.983	3.248
1.00	0.50	0.010	17.0000	-17.292	-16.709	0.330	0.861	0.664	2.792	3.039
12.00	0.50	3.000	15.0000	-24.694	-23.778	0.598	1.001	0.742	3.404	2.211
7.20	0.50	1.000	15.0000	-23.448	-22.587	0.588	1.002	0.735	3.327	2.933
5.20	0.50	0.500	15.0000	-22.603	-21.787	0.568	0.998	0.727	3.258	3.794
3.00	0.50	0.100	15.0000	-20.492	-19.773	0.473	0.955	0.704	3.082	3.891
2.50	0.50	0.050	15.0000	-19.458	-18.794	0.420	0.928	0.690	2.974	3.820
1.00	0.50	0.010	15.0000	-17.402	-16.824	0.336	0.880	0.667	2.796	3.752
12.00	0.50	3.000	12.0000	-24.866	-23.950	0.554	0.981	0.732	3.414	2.279
7.20	0.50	1.000	12.0000	-23.627	-22.764	0.548	0.985	0.725	3.340	3.150
5.20	0.50	0.500	12.0000	-22.786	-21.968	0.533	0.983	0.719	3.273	4.589
3.00	0.50	0.100	12.0000	-20.682	-19.966	0.448	0.946	0.697	3.090	5.406
2.50	0.50	0.050	12.0000	-19.648	-18.989	0.399	0.922	0.685	2.979	5.376
1.00	0.50	0.010	12.0000	-17.590	-17.019	0.318	0.880	0.663	2.798	5.382
12.00	0.50	3.000	10.0000	-25.088	-24.144	0.525	0.967	0.727	3.464	2.146
7.20	0.50	1.000	10.0000	-23.839	-22.950	0.523	0.973	0.720	3.390	3.060
5.20	0.50	0.500	10.0000	-22.988	-22.148	0.509	0.971	0.713	3.318	4.704
3.00	0.50	0.100	10.0000	-20.852	-20.132	0.422	0.932	0.688	3.105	5.940
2.50	0.50	0.050	10.0000	-19.810	-19.152	0.375	0.908	0.676	2.985	5.917
1.00	0.50	0.010	10.0000	-17.752	-17.181	0.299	0.868	0.656	2.804	5.806
12.00	0.50	3.000	8.0000	-25.269	-24.349	0.483	0.936	0.711	3.439	2.624
7.20	0.50	1.000	8.0000	-24.026	-23.153	0.480	0.946	0.705	3.373	3.526
5.20	0.50	0.500	8.0000	-23.178	-22.349	0.467	0.946	0.699	3.306	5.090
3.00	0.50	0.100	8.0000	-21.048	-20.335	0.386	0.909	0.676	3.098	6.067
2.50	0.50	0.050	8.0000	-20.012	-19.359	0.344	0.887	0.665	2.983	5.997
1.00	0.50	0.010	8.0000	-17.968	-17.397	0.276	0.850	0.646	2.811	5.794
12.00	0.50	3.000	5.0000	-25.699	-24.776	0.445	0.910	0.692	3.467	6.106
7.20	0.50	1.000	5.0000	-24.456	-23.584	0.421	0.908	0.683	3.386	6.080
5.20	0.50	0.500	5.0000	-23.608	-22.782	0.398	0.902	0.674	3.310	6.032
3.00	0.50	0.100	5.0000	-21.463	-20.753	0.323	0.862	0.651	3.100	5.816
2.50	0.50	0.050	5.0000	-20.401	-19.757	0.280	0.837	0.638	2.970	5.638
1.00	0.50	0.010	5.0000	-18.322	-17.774	0.215	0.792	0.615	2.770	5.229